

## REVIEW

[View Article Online](#)  
[View Journal](#) | [View Issue](#)



Cite this: *Energy Environ. Sci.*, 2019, 12, 2054

## Kinetic and material properties of interfaces governing slow response and long timescale phenomena in perovskite solar cells

Hongxia Wang, \*<sup>a</sup> Antonio Guerrero, \*<sup>b</sup> Agustín Bou, <sup>b</sup> Abdullah M. Al-Mayouf <sup>c</sup> and Juan Bisquert \*<sup>b</sup>

The last decade has witnessed the skyrocketing progress of perovskite solar cells (PSCs) with their current world record energy conversion efficiency reaching over 24%. Nevertheless, the unsatisfactory device stability and current–voltage hysteresis normally observed with most PSCs under operational conditions are the bottlenecks that restrict the application of this photovoltaic technology in practice. It is known that interface properties are at the heart of an electronic device's performance. Understanding the interactions occurring at the interfaces is important to design and develop effective strategies to address these issues associated with PSCs. In this review, we summarize the most recent advancement in understanding the interfaces in PSCs, in particular the interfaces of perovskite/electron transport layer (ETL) and perovskite/hole transport layer (HTL). Our main interest is to provide guidance on the immense complexity of dynamic behaviours of PSCs, particularly concerning the slowest time scale measurements that have a maximum impact on the actual operation of the solar cell. Therefore we address the separation of phenomena such as ion migration, interfacial charge accumulation, and surface electrochemical reactions. We provide an analysis of electrooptical small perturbation methods, including impedance spectroscopy (IS), and a description of negative capacitance, as well as spatially resolved techniques. The impact of different contacts with variable morphology and composition on the perovskite/ETL and perovskite/HTL interface properties reflected by the kinetics of charge transport and chemical reactions is discussed to provide deep insights into the operational mechanism of PSCs. We reach the conclusion that a number of measurements observed in the time frame of 0.1 to 10 s are due to the slow response of the ionic double layer, and we identify the asymmetric surface charge and discharge processes responsible for such kinetic effects. We also suggest the research direction regarding new approaches to understanding interfacial reactions of PSCs to achieve high device performance in the future.

Received 11th March 2019,  
Accepted 1st May 2019

DOI: 10.1039/c9ee00802k

rsc.li/ees

### Broader context

While metal halide perovskite materials have shown outstanding properties for applications in photovoltaics and optoelectronics, the operation of the devices is hindered by a number of phenomena that occur with extremely low frequencies and long times, and have proved very difficult to characterize systematically. Based on an extensive overview of contact phenomena we show that the interface of the perovskite material with organic or inorganic contacts is a site where a combination of ionic and electronic phenomena conspire to produce effects that severely modify the expectations received from traditional solar cell operation. Our analysis has three main aspects: the charge accumulation phenomena, the dynamic phenomena, and the physico-chemical features of the interface. From a review of a very broad range of methods and materials, we propose a general interpretation of the main factors dominating the response. In summary one can observe totally reversible phenomena of charge accumulation, a partial ionic binding that retards the response, and intense chemical interactions that perturb and invalidate the devices. Sorting out these phenomena is a key objective for ensuring stable performance and endurance in future technologies of metal halide perovskites.

<sup>a</sup> School of Chemistry, Physics and Mechanical Engineering, Queensland University of Technology, Brisbane, QLD 4001, Australia. E-mail: hx.wang@qut.edu.au

<sup>b</sup> Institute of Advanced Materials, Universitat Jaume I, 12006, Castello, Spain.  
E-mail: aguerre@uji.es, bisquert@uji.es

<sup>c</sup> Electrochemical Sciences Research Chair (ESRC), Department of Chemistry, Science College, King Saud University, Riyadh, Saudi Arabia

### 1. Introduction

Semiconductor materials based on metal halide perovskites have received enormous attention owing to their exceptional opto-electronic properties, which open applications in areas

such as solar cells, light emitting diodes, X-ray detectors, etc. The chemical formula of the perovskite can be described as  $\text{ABX}_3$  where A = monovalent cations such as methylammonium (MA), formamidinium (FA), and cesium (Cs), B = divalent cations such as lead (Pb), and tin (Sn) and X = halide anions including chloride (Cl), bromide (Br), and iodide (I).  $\text{MAPbX}_3$  was first synthesized by Weber in 1978.<sup>1</sup> The first attempt of applying methylammonium lead halide (bromide, iodide) ( $\text{MAPbBr}_3$ ,  $\text{MAPbI}_3$ ) in solar cells was reported by Kojima *et al.* in 2009, who employed the perovskite nanocrystals as light absorbers in a conventional sensitized solar cell using iodide/triiodide based liquid electrolyte.<sup>2</sup> The past ten years have witnessed the skyrocketing progress of the power conversion efficiency of perovskite solar cells thanks to advancement in material engineering and interface optimization. The current certified record efficiency of PSCs is 24% for single junction solar cells, which is comparable to crystalline silicon solar cells

and even surpasses the efficiency of thin film CIGS and CdTe solar cells. Compared to the solar cells based on light absorbers such as silicon, CIGS and CdTe, the most attractive features of PSCs include low temperature solution processing methods and high efficiency achieved with very thin layers (<500 nm), as well as the abundance of raw materials. These make them viable for large-scale production of light weight, flexible PSC devices using cost-effective methods such as roll-to-roll, screen-printing or slot-die, achieving low cost solar electricity in the future.

It has been well established that in addition to the excellent bulk photovoltaic (PV) characteristics, the interface properties determine to a large extent the performance of a hybrid perovskite solar cell (PSC) device. A typical PSC device architecture is composed of fluorine-doped tin oxide (FTO)/electron transport layer (ETL)/perovskite/hole transport layer (HTL)/gold, which contains four interfaces. Different interface materials used in



**Hongxia Wang**

*Assoc. Prof. Hongxia Wang is currently leading a research group at Queensland University of Technology (QUT) dedicated to development of new routes to enhance the performance and stability of next generation solar cells, in particular perovskite solar cells and energy storage devices such as supercapacitors through innovative material engineering and device engineering. She has published over 100 peer-reviewed research papers and some of her*

*papers are selected ESI high impact papers. She was the recipient of the “Australian Research Council (ARC) Future Fellowship”, and “Solar Energy Best Paper Award for 2016 in the topic of Photovoltaics” from the International Solar Energy Society.*



**Antonio Guerrero**

*Antonio Guerrero (PhD, University of East Anglia, UK) is contracted as a Ramon y Cajal fellow at the Institute of Advanced materials (INAM) in Castelló (Spain). He is specialized in the synthesis and characterization of semiconducting materials for their implementation in a variety of electrical devices. Over the last 5 years, his work has been mainly focused on three different lines of research: 1 - perovskite solar cells, 2 - organic photovoltaics and 3 - (photo)electrochemical cells. Overall, he is the author of more than 70 research articles, one book, one book chapter and he is the inventor of two patents.*



**Agustín Bou**

*Agustín Bou graduated in Physics from Universitat de València, Spain, in 2016 and joined the Institute of Advanced Materials of the Universitat Jaume I in Castellón, Spain, in 2017. His main topic of interest is the characterization and modeling of energy devices. His research has focused particularly on perovskite solar cells, focusing on impedance spectroscopy characterization and potential distribution and charge distribution modeling, including interface analysis.*



**Abdullah M. Al-Mayouf**

*Abdullah M. Al-Mayouf is professor of physical chemistry at King Saud University, Saudi Arabia and the director of the Electrochemical Sciences Research Chair (ESRC). His research interests focus on porous and nanomaterials, electrochemical methods, electrocatalysis and photoelectrocatalysis and surface modification. Currently, he is the editor-in-chief for Journal of Saudi Chemical Society.*

PSCs have been shown in recent reviews.<sup>3–6</sup> Moreover, it is often assumed that slow dynamic effects such as hysteresis in *j*–*V* curves are associated with ionic motion effects. However, a deterministic connection between the ionic displacement and the observed kinetic variations of the outer electronic current has not been established yet. In this review we will discuss the recent advances of understanding of the dynamic properties of PSC devices on the time scales associated with actual operation of the solar cell. We argue that the actuation of ions on the contact interface is a predominant cause of different types of slow kinetic effects. We further connect these dynamic effects with the chemical reactivity at the interfaces, which ultimately influences the device stability.

## 2. Timescales of ionic/electronic phenomena in PSCs

The first question we ask is about the transport rates in a PSC. And not only electronic transport, as it has been well established that a significant amount of ionic displacement influences the characteristics of measurement and operation of PSCs.<sup>7,8</sup> We are used to solar cells that are predominantly governed by electronic transport. For example, in silicon solar cells carrier transport is rather fast so that it is not likely to influence ordinary experimental observations, compared to recombination events.<sup>9</sup> This is why we can rely on energy diagrams that are determined with respect to a fixed background of ionic density.<sup>10</sup> On the other hand, in solar cells made of nanostructured metal oxide the electron transport is considerably slower and the transport resistance can be unambiguously determined.<sup>11</sup> In dye-sensitized solar cells diffusion of ions in the electrolyte often forms a prominent feature, but it can be neatly separated from electron transport components by measurement protocols.<sup>12,13</sup>

In a PSC, it has been found that many slow phenomena appear in physical measurements, the prominent representative being the hysteresis of current–voltage (*j*–*V*) curves.<sup>14–17</sup> Slow ionic transport is one possible reason for such a sluggish response.<sup>18</sup>



Juan Bisquert

*Juan Bisquert is a professor of applied physics at Universitat Jaume I de Castelló and the director of the Institute of Advanced materials (INAM). His main topics of interest are perovskite solar cells and solar fuel production. He has developed the application of measurement techniques and physical modeling that relate the device operation with the elementary steps that take place at the nanoscale dimension. He authored several books including Physics of Solar Cells: Perovskites, Organics, and Photovoltaics Fundamentals (CRC Press).*

*Physics of Solar Cells: Perovskites, Organics, and Photovoltaics Fundamentals (CRC Press).*

However, a clear connection between the rate of transport and the time response of PV properties has not been achieved, yet.

Recent work enables the quantification of ionic diffusion rates for lead halide perovskite materials, especially at room temperature. Methods such as the galvanostatic measurement,<sup>19</sup> impedance spectroscopy (IS), using the classical transmission line method,<sup>20</sup> and suppression of luminescence in laterally contacted electrodes,<sup>21</sup> have provided quantitative values of the diffusion coefficient of halide defects, which is on the order of  $D_{VI} = 1 \times 10^{-8} \text{ cm}^2 \text{ s}^{-1}$  for methylammonium lead trihalide perovskites (*i.e.* MAPbI<sub>3</sub> or MAPbBr<sub>3</sub>). In addition, cation transport has also been measured for extrinsic Li<sup>+</sup> and MA<sup>+</sup>. Alternatively, a variety of techniques operating in a wide array of frequency ranges have provided values of electronic mobility in metal halide perovskites.<sup>22</sup> While there is a scattering of values depending on many factors such as the specific composition and preparation methods of the perovskite materials, it is safe to take some representative values, which are indicated in Table 1.

The carrier conductivity (associated with the transport resistance) is the crucial quantity controlling possible power losses and determining which species govern carrier redistribution upon application of an external perturbation. A figure of merit that shows which current (either ionic or electronic) will be dominant in each situation is the quotient of conductivities. Considering electronic density *n* and ionic density *c* we expect that

$$\frac{\sigma_e}{\sigma_i} = \frac{n\mu_e}{c\mu_i} = 10^7 \frac{n}{c} \quad (1)$$

This result indicates that in any typical situation the current is mostly driven by electronic current, unless the density of mobile ions becomes many orders of magnitude larger than the electronic density. The latter may be expected in the dark in extremely low doped samples.

Starting from the previous general considerations, we may now compute several time constants that describe characteristic phenomena in hybrid perovskite materials. In order to establish the relative significance of transport phenomena on the kinetic timescale, it is necessary to choose a characteristic distance. A good point to start our analysis is to consider the kinetics of transport of ionic carriers across a region with a thickness of *d* = 100 nm. The transit time for each carrier to diffuse across such a distance is

$$\tau_{\text{diff}} = \frac{d^2}{D} \quad (2)$$

The results for a typical solar cell layer with a thickness on the order of hundreds of nanometers are shown in Table 2 and summarized in Fig. 1. For ionic transport, this will be the time needed for ionic carriers consisting of halide vacancies to cancel a new composition gradient that occurs under external variations, and it takes the value  $\tau = 10^{-2}$  s.

It is quite frequently found in PSC a much lower time scale for changes of variables like photovoltage or photocurrent.<sup>16</sup> Here this kinetic phenomenon with  $\tau = 10^0\text{--}10^2$  s is attributed to ionic double layer kinetics, as it will be discussed later on. Finally, another type of migration occurs on the time scale of

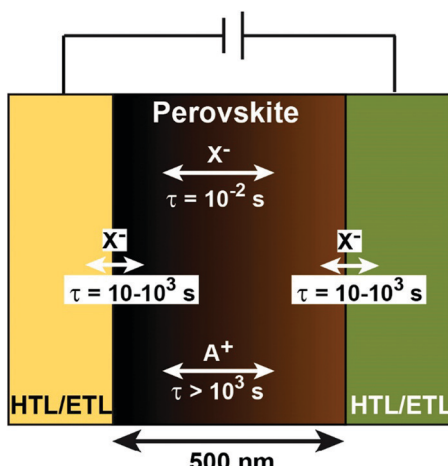
**Table 1** Some characteristic kinetic coefficients in PSCs based on  $\text{MAPbI}_3$  or  $\text{MAPbBr}_3$ , at room temperature

Type	Diffusion coefficient $D$ ( $\text{cm}^2 \text{s}^{-1}$ )	Carrier mobility $\mu$ ( $\text{cm}^2 \text{V}^{-1} \text{s}^{-1}$ )	Measurements <sup>a</sup>
Electron transport	0.3	$\sim 1\text{-}100$	Several methods like THzC, MWC, PLQ or SCLC <sup>22</sup>
Extrinsic $\text{Li}^+$	$1 \times 10^{-7}$	$4 \times 10^{-6}$	IS <sup>23</sup>
Halide vacancy transport ( $\text{V}_\text{I}^+$ )	$1 \times 10^{-8}$	$4 \times 10^{-7}$	Galvanostatic voltage measurement, <sup>19</sup> IS, <sup>20</sup> PL suppression <sup>21</sup>

<sup>a</sup> Representative techniques used to determine the mobility value: *i.e.* THzC: optical-pump-THz-probe photoconductivity, MWC: microwave conductivity, PLQ: PL quenching method, SCLC: space-charge limited current, IS: impedance spectroscopy.

**Table 2** Some characteristic timescales of kinetic phenomena in PSCs  $\text{MAPbI}_3$  and  $\text{MAPbBr}_3$ , at room temperature

Type	Time
Electronic transport across $d = 100 \text{ nm}$	$\tau = \frac{d^2}{D} = 10^{-9} \text{ s}$
Halide vacancy diffusion over a distance $d = 100 \text{ nm}$	$\tau = \frac{d^2}{D} = 10^{-2} \text{ s}$
The response of ions accumulated at the perovskite surface	$\tau = 10^0\text{-}10^2 \text{ s}$
Cation vacancy diffusion over a distance $d = 100 \text{ nm}$	$\tau = 10^3 \text{ s}$

**Fig. 1** Representative characteristic times for ionic phenomena in a typical perovskite solar cell.

many hours ( $\tau > 10^3 \text{ s}$ ), which can be associated with the much less mobile cation species (*i.e.*  $\text{MA}^+$ ).

### 3. Fast ionic transport in the bulk of the PSC

Ionic transport has emerged as a key player in perovskite research but its precise role in the slow response observed during electrical measurements and its relationship with degradation dynamics is under debate. On the one hand, there is strong evidence pointing to fast ionic transport in lead halide perovskites. An alternative measurement to the solar cell diode is a planar configuration with lateral contacts that provides a transport distance of hundreds of  $\mu\text{m}$ . In such a system the analysis of the PL by excitation at  $35 \text{ mW cm}^{-2}$  under an applied bias reveals the formation of a dark front that advances with time (Fig. 2).<sup>21</sup> Note that the applied voltage is similar to those at the maximum power point in working

PSCs. In addition, it is observed that the material becomes resistive as the dark front advances, indicating that doping is reduced in the dark area. Therefore, it is clear that techniques with spatial resolution are required to unambiguously correlate electrical measurements with the electronic/ionic response.

On the other hand, a careful analysis of the timescale of the ionic movement in the bulk of the perovskite layer highlights that ionic transport towards the interface cannot be the main reason that is responsible for the slow electrical response observed in PSCs (*i.e.* hysteresis). In particular, simultaneous analysis of the measured current during the previous PL experiment allows the calculation of the diffusion coefficient of the migrating iodine vacancies.<sup>21</sup> A value of  $D = 1 \times 10^{-7} \text{ cm}^2 \text{s}^{-1}$  leads to ionic transit times through a perovskite layer of  $100 \text{ nm}$  on the order of milliseconds. This ionic migration timescale has also been confirmed by another spatially resolved technique, transient Kelvin probe force microscopy (Tr-KPFM).<sup>24</sup> Alternatively,  $j\text{-}V$  measurements are carried out at scan rates that typically take several seconds. Therefore, it is clear that activated ionic transport in the bulk of the perovskite layer is only one requirement to observe hysteresis but not the main reason. Indeed, all evidence points to the chemical and physical interactions of these migrating ions with the external interfaces as the main reason for hysteresis observation. For example, a thin layer of PCBM placed on the top of  $\text{TiO}_2$  is able to completely suppress the measured hysteresis in the  $j\text{-}V$  response of devices with activated ion migration in the bulk of materials like  $\text{MAPbI}_3$ .<sup>25</sup> In the next section, we will describe the evidence for ionic accumulation at the surface of the PSC, and later we discuss the methods of observation of the kinetics of the surface charge.

### 4. Ionic effects at the interface

Under an applied bias ions rapidly reach the external interfaces with formation of an electrical double layer as it is well known in solid state electrochemistry. The combination of ionic and

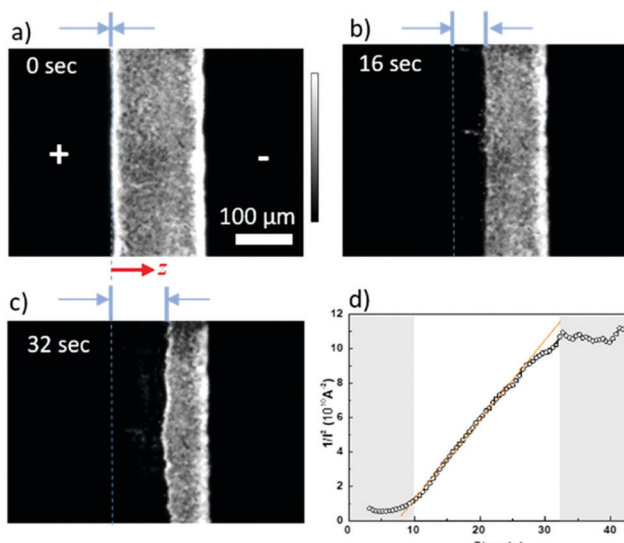


Fig. 2 (a–c) Time dependent PL images of a perovskite film  $\text{CH}_3\text{NH}_3\text{PbI}_{3-x}\text{Cl}_x$  measured under an external electric field of  $\sim 2 \times 10^4 \text{ V m}^{-1}$ , interdigitated configuration with a channel width of  $\sim 150 \mu\text{m}$ . (d)  $1/I^2$  monitored as a function of time during the measurement of experiment (a). Adapted with permission from ref. 21.

electronic phenomena such as space charge, interfacial electron transfer and ionic reactivity leads to several possible types of physical and chemical interactions at the interfaces. There are different time resolved electrical techniques that can be used to decouple ionic and electronic responses, such as impedance spectroscopy, which has been widely used in PSCs. For example, a pure ionic contribution with the classical transmission line for ion migration is observed during the measurements of  $\text{MAPbBr}_3$  monocrystals (Fig. 3a). This technique measures the electrical response in the frequency domain separating resistive and capacitive contributions (or charge accumulation). A useful method to represent the impedance data is the complex impedance plot where the  $x$ -axis ( $Z'$ ) is related to resistive elements and the  $y$ -axis ( $-Z''$ ) to capacitive elements. A resistive element connected in parallel to a capacitor (RC) leads to an arc in the complex impedance plot. The most common feature in the impedance spectra of a PSC is the appearance of two arcs as shown in Fig. 3b. The data can be fitted to the equivalent circuit shown. Both resistances  $R_1$  and  $R_2$  correspond to losses from both bulk and interfacial recombination.<sup>19</sup> Moreover, both have the same trends as a function of photovoltage or light intensity, indicating that they have a common origin. In contrast, the source of capacitances is clearly different. The capacitance-frequency ( $C-f$ ) plot of the IS data is very useful to understand the capacitive contributions and correlate the charge accumulation with the characteristic time of the physical process. It has been established that there are two plateaus indicating well-differentiated capacitances in the  $C-f$  plot of PSCs, Fig. 3b. The high frequency capacitance  $C_g$  is the dielectric capacitance,<sup>26</sup> related to the bulk polarization, and the low frequency capacitance  $C_s$  corresponds to surface accumulation processes.<sup>21</sup> The fact that  $C_s$  changes when different contacts configurations

are used is strong evidence for the existence of a surface capacitance. A similar behaviour is observed in perovskite quantum dot films.<sup>27</sup>

The features of low frequency capacitance in metal halide PSCs have been broadly studied and a general characteristic picture has emerged. The fact that ions migrate across the bulk under a voltage bias or light soaking is well known. When ions arrive at the interfaces, they accumulate there. A main component of the double layer is the Helmholtz layer, formed by the ions in contact with the electrode surface, which provides a capacitance of the order of  $10 \mu\text{F cm}^{-2}$ . However, there also is a diffuse double layer, which contains a surface charge<sup>29</sup>

$$C_{\text{diff}} = \frac{2\epsilon\epsilon_0 k_B T}{qL_D} \sinh\left(\frac{q\Delta\phi}{2k_B T}\right) \quad (3)$$

This charge is distributed on the typical distance of a Debye length for the electrode surface,

$$L_D = \left(\frac{\epsilon\epsilon_0 k_B T}{q^2 N}\right)^{1/2} \quad (4)$$

In eqn (3) and (4) the standard symbols have their usual meaning.<sup>30</sup>  $\Delta\phi$  is the potential drop across the double layer, and  $N$  is the net underlying ion density in the bulk.

Zarazua *et al.*<sup>28,31,32</sup> showed by analysis of the evolution of  $C_s$  with  $V_{\text{oc}}$  that the surface capacitance  $C_s$  is actually an accumulation capacitance, however, it depends on the accumulation of both ionic and electronic carriers and is highly dependent on the specific binding of the perovskite to the contact surface. In this line, direct evidence for the intimate connection between surface capacitance and hysteresis emerged by comparing normal and inverted versions of PSCs as indicated in Fig. 4a.<sup>33</sup> The cells with a PCBM electron contact display a much lower low frequency capacitance than those with a  $\text{TiO}_2$  contact. And correspondingly,  $j-V$  cycling hysteresis is significantly reduced in the inverted cell. Further evidence for this strong correlation has been obtained by measuring dark currents at different scan rates as shown in Fig. 4b and c.<sup>34</sup> By modification of the device configuration it is possible to suppress the capacitive contribution of the current. The square-like response is removed in a configuration that avoids the use of a metal oxide based ETL (Fig. 4c). This is further confirmation that the surface capacitance is a composition of ionic and electronic carriers accumulated at the interface and highly depends on the contact interfaces of the perovskite/charge extraction layer.

The rise of capacitance at low frequency has been interpreted in many cases as the manifestation of bulk traps. However a recent study<sup>35</sup> using the analysis of low frequency noise has found that the capacitance does not scale with thickness, in agreement with the previous scaling properties obtained by impedance spectroscopy.<sup>36</sup>

Metal oxide based ETLs typically lead to large surface capacitances and hysteresis as shown above. The impact of the  $\text{TiO}_2$  compact layer thickness on the hysteresis behavior of carbon based HTM-free PSCs was confirmed by Han *et al.*<sup>37</sup> By tuning the thickness of the spray-deposited  $\text{TiO}_2$  layer over a

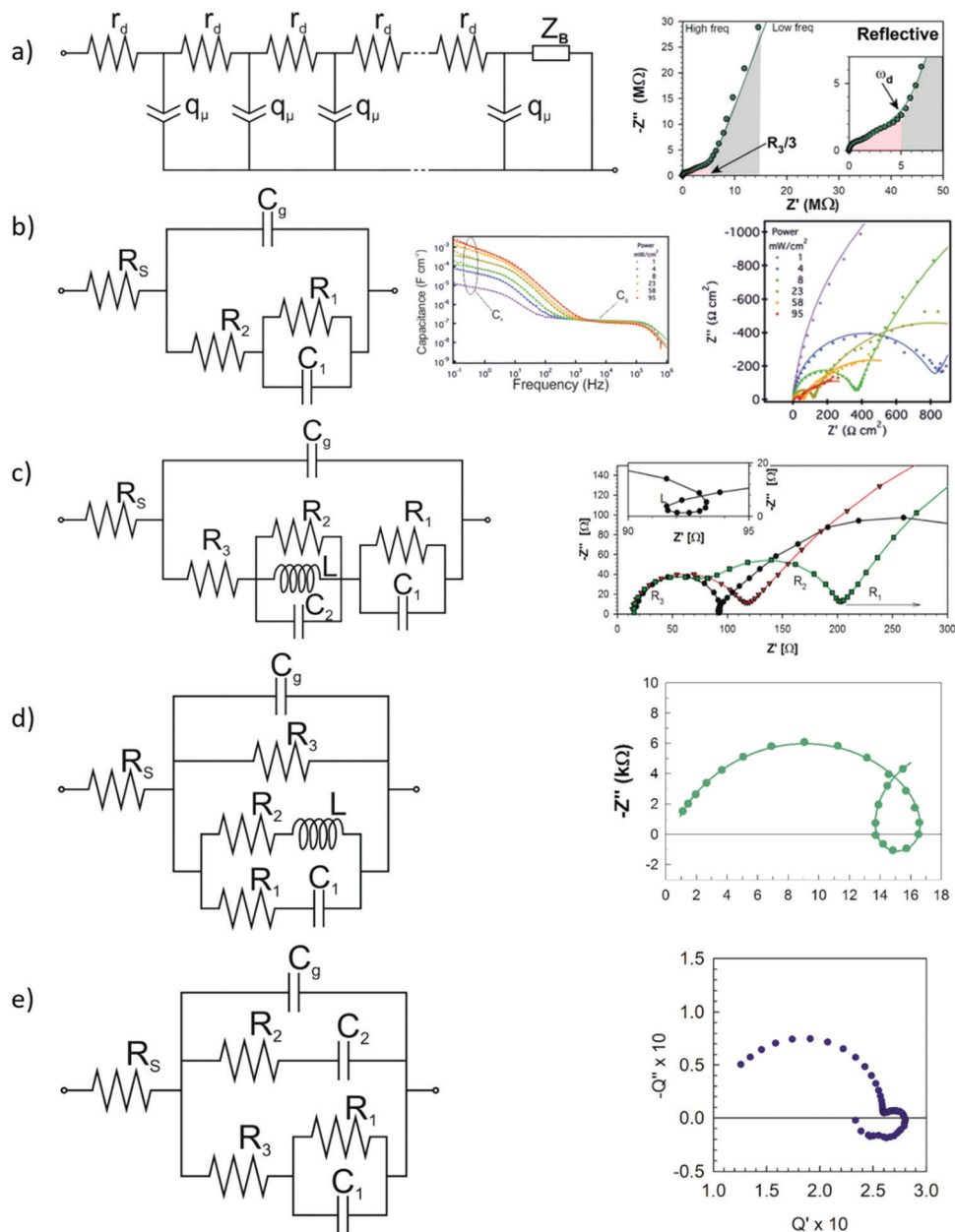


**Fig. 3** Summary of equivalent circuits used for the analysis of impedance spectra of perovskite solar cells with examples of representative spectra for each circuit. Here, we use the following notation for capacitances:  $C_g$  is the geometrical capacitance,  $C_1$  is the low frequency capacitance usually associated with accumulation, and  $C_2$  is the intermediate frequency capacitance; and for resistances:  $R_s$  is the series resistance, and  $R_1$ ,  $R_2$  and  $R_3$  are always ordered from the lowest frequency resistance to the highest, starting from 1. (a) Transmission line showing the impedance of ion diffusion in a finite layer used for ionic transport quantification in perovskites, highlighted in red. Reproduced with permission from ref. 20. (b) Equivalent circuit used for two arc spectra. Here we show capacitance spectra depending on light intensity. Reproduced with permission from ref. 28. (c) Equivalent circuit used for three arc spectra and intermediate frequency loops; here, resistances appear in series. Reproduced with permission from ref. 31. (d) Equivalent circuit used for spectra with two arcs that vary in concordance which have exotic features such as inductive loops or negative capacitances; here, resistances appear in parallel. Reproduced with permission from ref. 64. (e) Equivalent circuit obtained from the analysis of both IS and IMPS data together; here we have resistances in parallel as well as in series. Reproduced with permission from ref. 79.

few nanometers, the hysteresis behavior of the perovskite was switched from inverted to hysteresis-free and then to normal (Fig. 5). The combined effects of the dynamics of charge accumulation and charge recombination are believed to be responsible for the observed behavior.

The dependence of capacitance on frequency in organometal halide perovskites shows a range of features as discussed before, but it has been concluded that the low frequency domain is mainly associated with the surface capacitance. It is therefore expected that slow kinetic changes of the surface

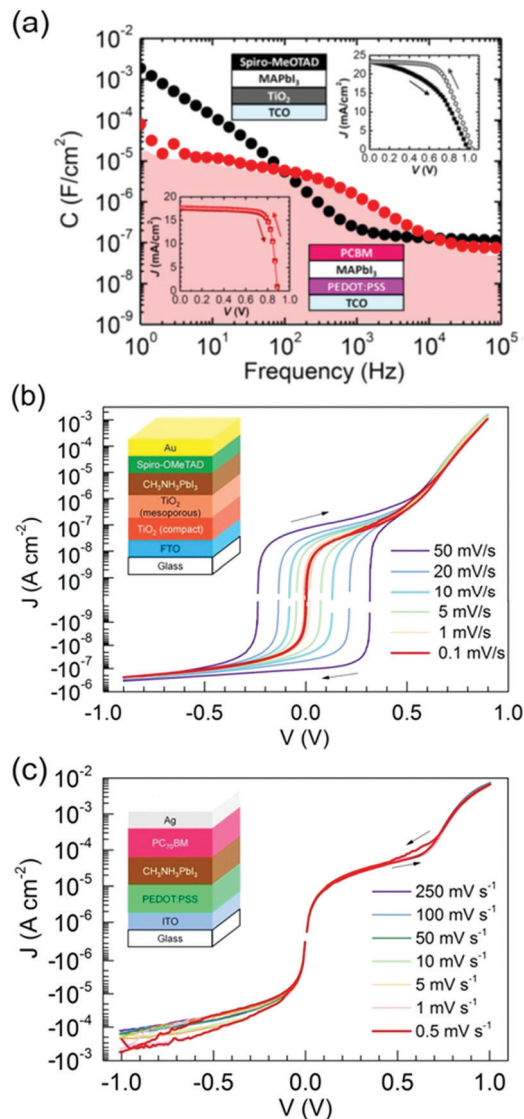


**Fig. 4** (a) Capacitance–frequency plot under one sun illumination under short-circuit conditions (bias voltage = 0 V). The normal and the inverted structures represent cp-TiO<sub>2</sub>/MAPbI<sub>3</sub>/spiro-MeOTAD and PEDOT:PSS/MAPbI<sub>3</sub>/PCBM, respectively. Reproduced with permission from ref. 33. (b and c) Dark  $j$ – $V$  curves measured at different scan rates with corresponding structures sketched in the insets. The positive currents are the forward bias direction. Reproduced with permission from ref. 34.

will provide measurable evolution of the capacitance value. Garcia-Belmonte and coworkers have been able to identify the surface depletion layer capacitance and the subsequent Mott–Schottky plot.<sup>38</sup> However, they have found that the surface depletion layer capacitance is affected by a large extent of hysteresis when the applied voltage undergoes a scan cycle (Fig. 6). These results are important as they reveal the electrical response in proximity to the contact, and this is a manifestation of surface attached species, *i.e.*, a change of surface charge that occurs on a much longer scale than the measurement of the capacitances.<sup>39</sup>

In summary, once the ions complete the accumulation, their responses to the small perturbation are slow, with characteristic times related to the low frequency capacitance. In a later section we argue that this surface polarization takes longer to be discharged than the time it takes for charging, a phenomena connected to surface attachment and electrochemical surface reactions.

Due to the complexity of the surface phenomena it is important to adopt complementary measurement techniques that may validate specific assumptions. Photoluminescence (PL) measurements of more simple configurations containing only one perovskite/contact interface can also unveil information on the properties of the perovskite/external contact interfaces. In early work, it was found a large drift of PL intensity that persists over 20 s.<sup>16</sup> Measurements by Lundt *et al.*<sup>40</sup> revealed dramatic modifications of PL depending on the treatment of the exposed perovskite surface (Fig. 7). Significant PL quenching occurs with the deposition of 1 nm C<sub>60</sub>, which could be interpreted as passivation of surface traps. However, a similar effect occurs when using an amorphous thin organic buffer layer between the perovskite and the C<sub>60</sub> but not when the thin layer is used without C<sub>60</sub>. Therefore, the PL quenching is attributed to the formation of space charge, which is associated with electron capture in C<sub>60</sub> and compensating ions on the perovskite side.

Recently, the critical effect of ions present at the ETL/perovskite interface has been highlighted for a wide band gap perovskite based on MAPbBr<sub>3</sub>.<sup>41</sup> The ETL was treated with additives containing Li<sup>+</sup> to reduce undesired interfacial recombination processes at the MAPbBr<sub>3</sub>/TiO<sub>2</sub> interface.

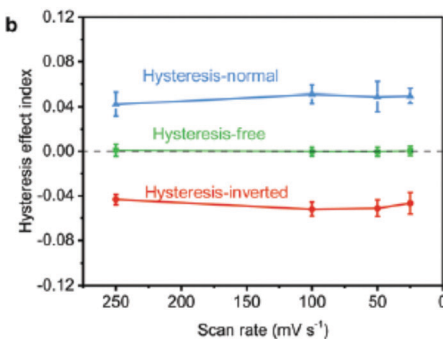


**Fig. 5** Dependence of the hysteresis effect index on (a) c-TiO<sub>2</sub> layer spray deposition cycles and (b) scanning rates for hysteresis-normal, hysteresis-free and hysteresis-inverted devices. Reproduced with permission from ref. 37.

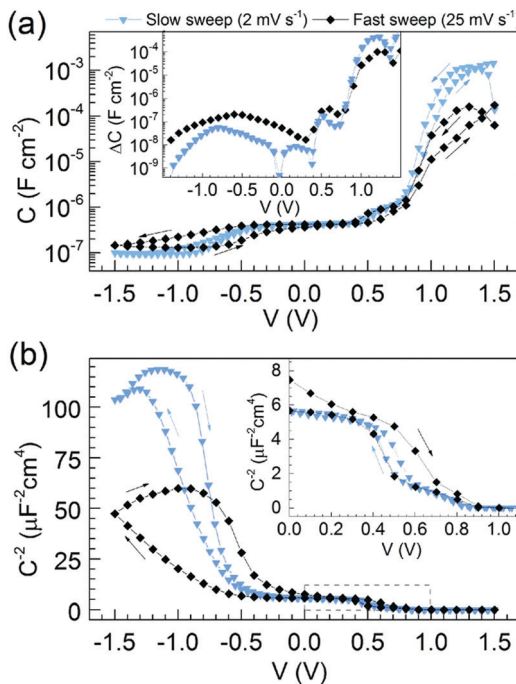


**Fig. 6** (a) Capacitance–voltage curve and (b) respective Mott–Schottky plot of a  $\text{CH}_3\text{NH}_3\text{PbI}_3$ -based PSC with a mesoporous  $\text{TiO}_2$  matrix for a larger DC bias window at different scan rates, as indicated. Inset in (a): the corresponding capacitance absolute difference between scan directions  $\Delta C$ . The inset in (b) is the typical Mott–Schottky plot region, shown inside the dashed gray square. Reproduced with permission from ref. 39.

An emission peak at 670 nm (Fig. 8) was identified with interfacial recombination from the  $\text{TiO}_2$  to the perovskite layer, which could be suppressed by doping the  $\text{TiO}_2$  with a salt containing  $\text{Li}^+$ . It was proposed that the presence of  $\text{Li}^+$  ions at the ETL increases the cation density at the hole accumulation zone, thus increasing the size of the space charge layer. Therefore, the surface density of electronic holes at the critical zone of the surface of the  $\text{TiO}_2$  layer is reduced, as indicated by the decrease of charge-transfer radiative recombination observed at 670 nm and the simultaneous increase in the band-to-band emission of the perovskite.

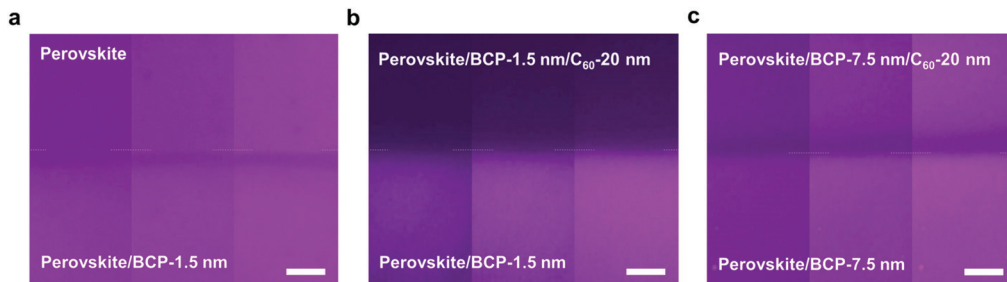


**Fig. 7** Time-resolved fluorescence microscopy images of perovskite films with (a) bare perovskite, (b) a 1.5 nm amorphous buffer layer spacer with 20 nm  $\text{C}_{60}$ , and (c) a 7.5 nm buffer layer spacer with 20 nm  $\text{C}_{60}$ . The buffer layer-only coated perovskite film is provided in each panel for reference. The time scale is 0 s (left), 30 s (middle), and 60 s (right) for each figure; the brightening of the PL with time stems from space-charge accumulation, which increases radiation recombination rates. The dashed line is used as a guide to the eye to indicate the interface position. The scale bar is 100  $\mu\text{m}$  for all figures. Reproduced with permission from ref. 40.

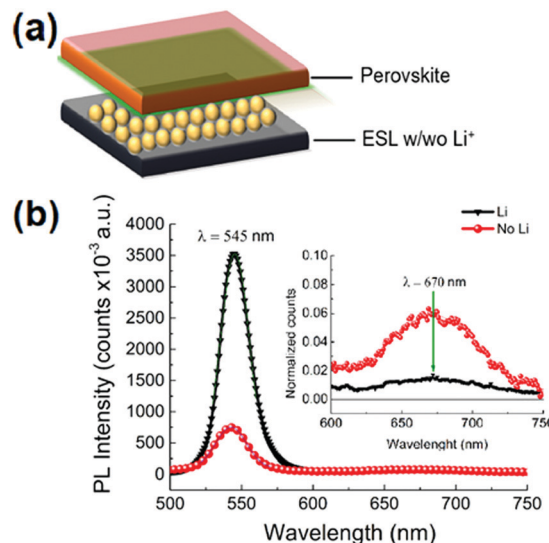


**Fig. 8** Photoluminescence measurements focused on both the  $\text{TiO}_2$  and perovskite showing the enhancement of perovskite emission and suppression of the interfacial emission. PL spectra obtained under continuous wave (CW) excitation ( $\lambda_{\text{exc}} = 380 \text{ nm}$ ,  $I_{\text{exc}} = 10 \text{ mW cm}^{-2}$ ) of devices with (black) and without (red) lithium treatment at the metal oxide contact. The inset plot shows the quenching of the second feature when lithium is present at the metal oxide contact. Reproduced with permission from ref. 41.

Reduced recombination was confirmed by IS and electroluminescent measurements.

## 5. Electronic effects at the interface

Although ionic effects have grabbed attention in the perovskite community because of their peculiarity, electronic phenomena remain key for improving device performance. While bulk electronic phenomena such as carrier diffusion or bulk recombination are well established advantages of perovskite materials,<sup>42</sup> interfacial phenomena such as traps, surface recombination and charge extraction remain a big issue to completely achieve high and stable performance.<sup>43</sup> Thus, choosing adequate materials as extraction layers is a crucial issue.

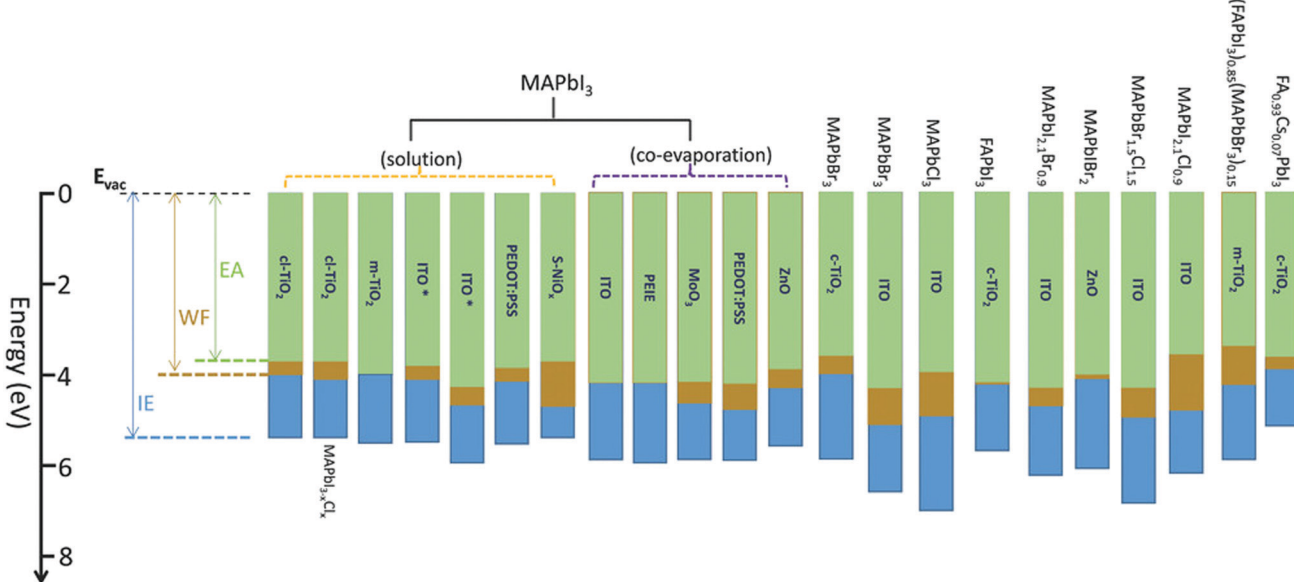


**Fig. 9** WF, IE, and EA values for various perovskites reported by different groups, which are prepared either on different underneath layers and/or by different methods. The listed materials on the bars are the substrates, and the types of perovskite materials are listed on top. WF and IE are derived from UPS measurements, while EA values are derived from the transport gap or optical bandgap. The star symbols (\*) represent that the work used the same preparation method and the same substrate material but reported in different literature. Reproduced with permission from ref. 48.

When selecting a material for extracting carriers, energy level alignment provides a dominant criterion to produce a good selective contact.<sup>44,45</sup> In the case of perovskites, this is not an easy question, since the energy level of the perovskite itself is strongly dependent on the composition (*i.e.* different halides or cations), surface termination,<sup>46</sup> the surface state charging,<sup>47</sup> and even on the preparation method.<sup>48</sup> Actually, perovskite energy levels may change depending on the substrate on which they are prepared, as shown by Miller *et al.* using photo-emission spectroscopy.<sup>49</sup> In fact, substrates may change doping densities and may turn the perovskites from n-type to p-type. Both for the ETL and the HTL, there are some materials that have been widely used because of their suitable properties, Fig. 9.

On the one hand, for the ETL there are two main options, metal oxides (such as TiO<sub>2</sub>, SnO<sub>2</sub> or ZnO) and organic layers (such as C<sub>60</sub> or PCBM). In the case of metal oxides, TiO<sub>2</sub> is the one that has been more widely used, giving high efficiencies both in planar and mesoporous layers. However, the TiO<sub>2</sub>-perovskite interface has given substantial problems like charge accumulation<sup>32</sup> and hysteresis.<sup>14</sup> Despite a good energy level alignment, charge extraction problems, surface non-radiative recombination and charge accumulation have been found to limit the device performance. Partial solutions to those problems have been found *via* TiO<sub>2</sub> doping with different materials. Liu *et al.* reported hysteresis free PSCs by doping TiO<sub>2</sub> with lithium, reducing the density of electron traps and increasing the conductivity.<sup>50</sup> Tan *et al.* proposed contact passivation by using a chlorine capped TiO<sub>2</sub> colloidal nanocrystal film, reducing interfacial recombination.<sup>51</sup> In general, contact modification of TiO<sub>2</sub> is needed to suppress undesired interfacial processes *via* doping or passivation.<sup>52–54</sup> The ETL-perovskite

band alignment is really sensitive to all the electronic processes that occur at the interface, and may change the interface capacitance by some orders of magnitude.<sup>55</sup> Extended information about the chemical modifications of the contact is provided in Section 9.

The hypothesis of surface electronic traps causing hysteresis<sup>43</sup> is difficult to distinguish from ionic binding or surface polarization and relaxation effects, since surface capacitances would be high as well in the case of surface electron traps. However, some changes of ionic species affect strongly the capacitance onset over the Helmholtz layer, and it seems unlikely to invoke a passivation of traps to explain such an effect.<sup>41</sup> The predominance of an electrostatic effect caused by the ion distribution has been explicitly shown using ultrathin buffer layers in PL experiments, as shown in Fig. 7.

On the other hand, two main materials are used for the HTL side generally: spiro-OMeTAD and PEDOT:PSS, although there is ongoing research into finding suitable materials, which are usually organic. As commented on before, the perovskite energy levels change with the perovskite composition. These changes are significant in the perovskite valence band, but the conduction band changes are smaller. It is then important to change the HTL characteristics to get good band alignment.<sup>56</sup> One of the reasons why spiro-OMeTAD is widely used is the fact that it allows energy level changes by oxidation, thus being a versatile option.<sup>57</sup> Gelmetti *et al.* recently analyzed the behaviour of different organic HTLs with chemical structures similar to those of spiro-OMeTAD but different energy levels, and demonstrated that the HOMO energy values differ significantly when depositing on top of the perovskite layer, having an impact on the  $V_{oc}$ , which justifies the difficulties in finding an appropriate HTL material.<sup>58</sup> Nevertheless, problems with the perovskite-HTL

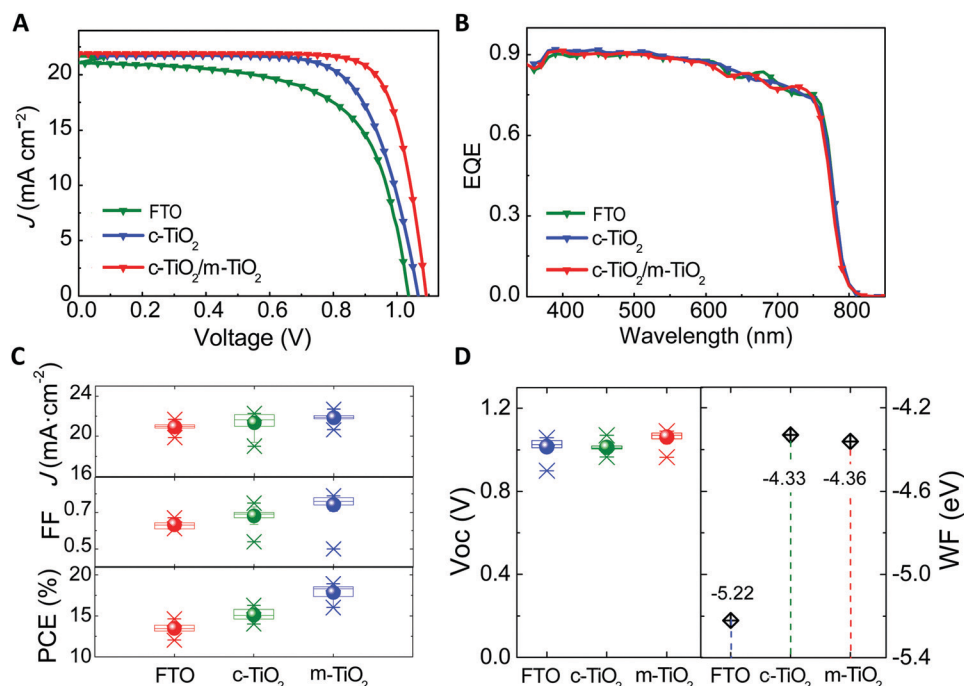


**Fig. 10** (A) Current–voltage ( $j$ – $V$ ) curves measured under 1 sun illumination and (B) external quantum efficiency (EQE) of representative perovskite solar cells containing meso- $\text{TiO}_2$ , c- $\text{TiO}_2$  and ETL-free architectures. (C) Summary of device parameters obtained for more than 40 cells measured under AM1.5G sun illumination, room temperature and air conditions. (D) The open circuit voltage in comparison to the work function of the different contact layers are also indicated for comparison (right panel). Reproduced by permission from ref. 59.

interface also relate to reactivity and degradation in addition to energy level alignment, and this is discussed further in a later section.

A classical question about PV operation mechanisms is whether the work function difference between the electron and hole contact materials correlates with the open circuit voltage. Energy alignment at the contact is important to produce a good selective contact, but once this is achieved, the local adaptation in the contact region makes  $V_{\text{oc}}$  quite independent of the overall built-in voltage. A striking demonstration<sup>59</sup> is presented in Fig. 10, where cells with widely different work functions at the ESL show very similar PV characteristics, mainly differing in the FF.

## 6. Dynamic effects and time constants

In Section 4 we have outlined several phenomena that point to the strong experimental manifestation of accumulation of ionic and electronic charge in the contacts of the device. The interface of the perovskite with the contact appears to be a critical site controlling these phenomena. In order to classify and understand these interfacial phenomena it is important to attribute an interpretation to kinetic constants that describe the changes of the surface conditions, in the context of a variety of phenomena indicated in Table 2.

A brief light soaking treatment produces drastic changes in the open circuit voltage decay (OCVD) as shown in Fig. 11.<sup>60</sup> In these experiments the  $V_{\text{oc}}$  of the device is monitored after the

light is turned off for different pre-treatment light soaking times ( $\Delta t$ ). The effect of light seems to be similar to that observed under a voltage bias stimulus. The OCVD is slow for a device that has not been light soaked previously and as expected for a solar cell the devices are able to obtain a null  $V_{\text{oc}}$  in the dark. Alternatively, a device that has been light soaked shows a fast  $V_{\text{oc}}$  decay, but a persistent potential remains in the device, indicating that migrating ions interact with the external contacts to create an electrostatic potential. The construction of an additional voltage that persists on a long time scale is attributed to the partial attachment of cations to the surface during the short treatment of pre-illumination.

The energy diagram at the  $\text{TiO}_2$ /perovskite contact at four different stages of the illumination condition shown in Fig. 12 indicates a microscopic interpretation of the changes occurring at the interface and the associated observation of the cell voltage. For fresh devices measured in the dark and for light soaking experiments using short times ( $\Delta t = 1$  s) band bending is related to a depletion layer at the perovskite region close to the  $\text{TiO}_2$ , leading to flat bands under open circuit conditions under illumination. Under light soaking conditions, migration of positive cations and iodine vacancies is induced, generating an accumulation regime at the interface. The combination of the ionic charge and hole concentration at the perovskite side of the interface forms an electrostatic potential as a result of the electric field across the interface. This potential is added to the built-in potential, and persists for a considerable time when the illumination is suppressed due to ions remaining in the double layer region. The structure of surface polarization considering a

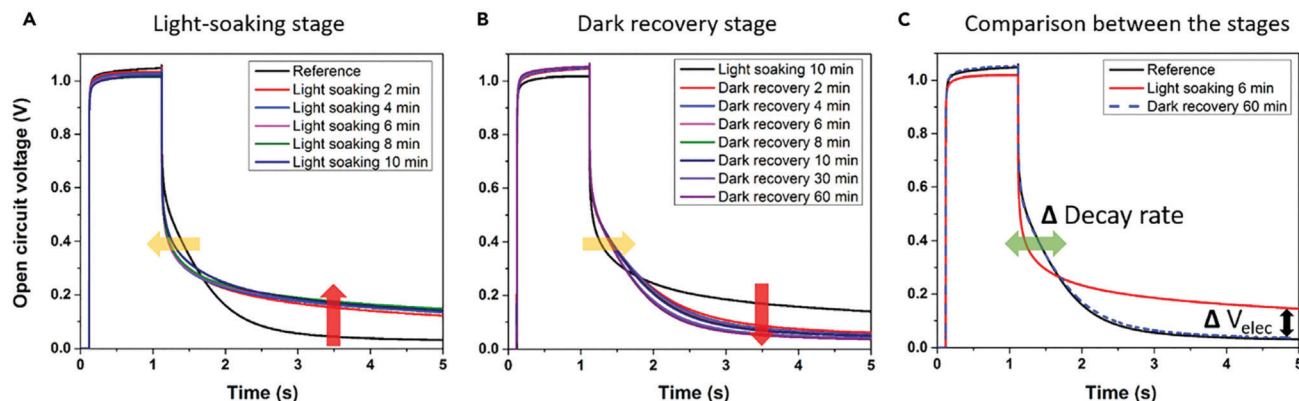


**Fig. 11** Top row: open circuit voltage decay (OCVD) data for a PSC with a  $\text{TiO}_2/\text{CH}_3\text{NH}_3\text{PbI}_{3-x}\text{Cl}_x$  interface. (A and B) Changes in the decay rate appear in the light-soaking stage (A) and slowly revert back during the dark recovery stage (B). (C) An exemplary comparison of three OCVD measurements that show the two photo-induced changes in the decay rate and the buildup of an electrostatic potential,  $V_{\text{elec}}$ . Reproduced with permission from ref. 60.

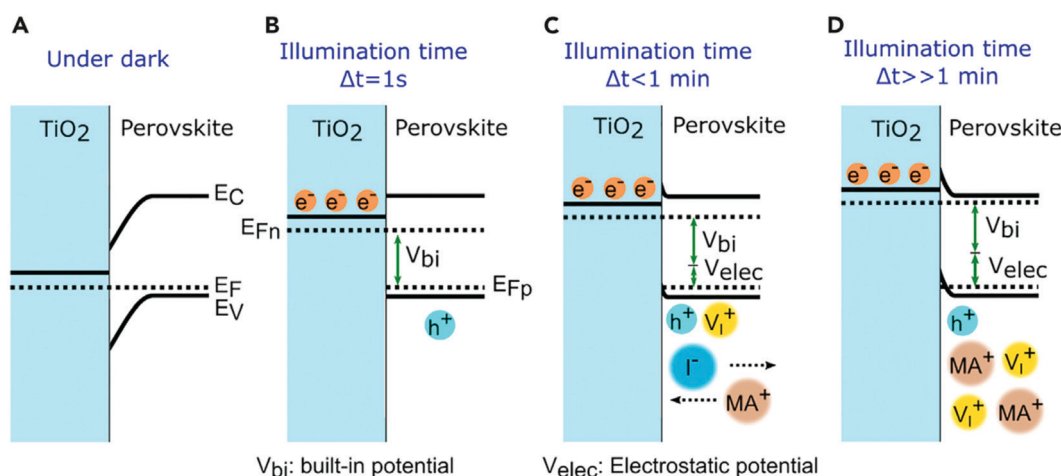


**Fig. 12** The energy diagram at the  $\text{TiO}_2/\text{perovskite}$  contact at four different stages. (A) In the dark. (B) At a very short illumination time of  $\Delta t = 1 \text{ s}$ . (C) At an illumination time close to 1 min. (D) After a substantial illumination time of  $\Delta t > 1 \text{ min}$ . This potential is added to the built-in potential. Reproduced with permission from ref. 60.

combination of electronic and ionic mobile species can be established by a proper numerical analysis.<sup>61</sup> The role of ions in the formation of accumulation layers needs to be quantified to know the structure of the energy diagrams across the PSC. A study with different HTL shows that a good alignment not only suppresses the hysteresis, avoiding charge accumulation at the interfaces, but also degradation of the hole transport layer is reduced.<sup>62</sup>

An electrical model that relates the surface polarization and the electrical response during the  $j$ - $V$  measurements has been developed.<sup>63</sup> The scan from forward to reverse voltage produces a bump in the current due to the slow release of the surface attached charge. This is described by an equation of the type

$$\frac{dV_s}{dt} = -\frac{V_s - (V - V_{\text{bi}})}{\tau_r} \quad (5)$$

Here  $V_{\text{bi}}$  is the built-in potential across the initial barrier,  $V_s$  is a surface voltage related to the internal surface charge (ions and holes), and  $\tau_r$  is the relaxation time associated with the equilibration of the interface to the external voltage, which is

mainly regulated by the ion kinetics as already described in relation to the open circuit voltage decay above. A similar approach has been used to account for the observation of impedance loops in the IS spectra, and it is shown in Fig. 3d.<sup>64</sup> The simulations with this circuit generate impedance spectra typical for PSCs, two arcs and accumulation capacitance  $C_s$ , and new exotic features: inductive loops and negative capacitances which are related to the sluggish ion movement that retards the surface polarization response. This is due to autonomous relaxation of the internal voltage, eqn (5), that generates the inductive dynamics. The results of both surface polarization model fitting of  $j$ - $V$  curves and equivalent circuit analysis by the model in Fig. 3d show a very good agreement that establishes  $\tau_r$  on the order of 20 s for measurements of different types of PSC at room temperature.

It was previously reported that negative capacitance effects are rather sensitive to the surface conditions,<sup>65</sup> and a very large inductive effect was obtained in composite interfaces.<sup>66</sup> Recently other studies have also stressed the connection of

ionic-electronic accumulation at the surface, and its possible influence on electron transfer and recombination rates, in order to explain large capacitance and inductive behaviour.<sup>67–69</sup> In the same spirit it was previously suggested that recombination is affected by ions.<sup>70</sup> Concerning the complexity of the impedance spectroscopy response of perovskite solar cells, these approaches are focused in the right direction in providing explanations combining ionic and electronic features; however, the models remain at a fuzzy stage, therefore important physical details cannot be verified yet. One study has provided a confirmation of negative capacitance<sup>68</sup> using older arguments for the inductive response in the time domain.<sup>71</sup> It is worthwhile to mention that earlier approaches based on charge collection and modification of the built-in electrical field in the bulk appeared to be abandoned in favor of the predominance of charging and reaction effects at the interface. Nevertheless, it must be remarked that capacitive features have to be explained in the frequency domain, as we need models that fit the IS data and produce quantitative conclusions. Indeed the recognized power of IS consists of the ability to use the spectra to separate features that cannot be well distinguished in the time domain. Therefore we need more spectral analysis, rather than less.

The topic of negative capacitance is an important part of the behaviour of many solar cell devices analyzed in the frequency domain.<sup>72</sup> “Negative capacitance” and “inductive behaviour” are widely accepted synonyms of a type of spectral behaviour, but the main effect associated with it, not so frequently noted, is that the resistance becomes smaller as the frequency decreases, causing the famous loops in the impedance spectra. This effect most often goes in the direction of decreasing the solar cell performance, particularly in perovskite solar cells,<sup>73</sup> and needs to be explained even on practical grounds.

However, this research topic is plagued by a basic problem. It is relatively easy to make some models that produce negative capacitance. There are some basic resources, which basically consist of introducing a cross-dependence in any regular electrochemical or semiconductor device model.<sup>74,75</sup> To implement the method you make a rate constant depend on voltage, or you make one element in a circuit depend on the current elsewhere (there are endless possible variations), and in the small perturbation model you obtain a dephasing of the ac current and voltage in which the model cannot be described by regular capacitors and resistors. In fact in such a model the “capacitance” (as defined by the imaginary part of the impedance  $Z$ ) can become very large, or negative, the resistance decreases at low frequency, and several things can happen, while causality holds. The reason is that such tricks, which represent very real phenomena in far from equilibrium situations, abandon the central diktat of detailed balance: the rule that the transition rates in nonequilibrium should be the same as those of equilibrium.<sup>76</sup> The cross-correlations introduced in the physical model violate this rule, thus thermodynamic quantities such as the capacitance lose their ordinary meaning in the out-of-equilibrium situation. This is one reason why it is so easy to find “explanations” of the negative capacitance, and at the same time it is rather demanding to demonstrate experimentally a given coupling mechanism in such complex systems.

One promising approach is to combine different frequency modulation methods such as IS and IMPS, as these should give complementary spectral information that may reveal specific mechanisms.<sup>77</sup> For normal models obeying detailed balance, it was shown by Bertoluzzi and Bisquert that all these methods reduce to a common model that describes the different spectral responses.<sup>78</sup> In principle it appears that one method only should confirm the result of the other. However, a recent study by Ravishankar *et al.*<sup>79</sup> reveals an interesting outcome of this approach, see Fig. 3e. It was shown that the spectral coupling of resistances and capacitances is rather different in the separate IS and IMPS spectra. Therefore, IMPS can reveal three physical processes in cases where IS only shows two, due to the overlap of the effects of the separate contacts. This route will enable one to obtain further information about the meaning of the low frequency resistances, in combination with complementary techniques.<sup>35</sup>

Nevertheless, the previous characterization methods suffer from the limitation that all the information is obtained from the physical measurement at the external contacts, without real internal spatial resolution. Thus it is important to adopt complementary methods. One important study by Weber and coworkers<sup>80</sup> of the distribution of charge carriers by Kelvin Probe Force Microscopy (KPFM) provided a direct demonstration of the strong ionic-electronic accumulation at the perovskite/TiO<sub>2</sub> contact, so that this is a fact that cannot be denied anymore. This was followed by a detailed time transient study indicated in Fig. 13.<sup>24</sup> They measured the time scale that is needed for charge redistribution of PSCs under operational conditions and have found that the formation of localized interfacial charge occurred in a short time of 10 ms under illumination. However, after the light is switched off, the interfacial charge can stay over 500 ms, which creates a slow response of the photocurrent transient. A further detailed analysis of the contribution of ions and electronic charge shows that the role of slow mobile ions in the  $j$ - $V$  hysteresis is quite small. Instead, the hysteresis is mainly caused by formation and desorption of interfacial charges.<sup>24</sup> Another important result of this paper is the explanation of a potential gradient related to the electrical field as shown in Fig. 13b. Weber *et al.* showed that such a potential distribution corresponds quantitatively to the tail of the double layer, as shown in eqn (3), extended into the bulk due to a Debye length on the order of 200 nm, corresponding to a background charge density of  $10^{15}$  cm<sup>-3</sup>, in excellent agreement with previous results of transient charging current.<sup>29</sup> The potential distribution along the bulk is an equilibrium feature, and the dominant kinetics is that of charging the interface.

It should be mentioned that the very strong, well-recognized transient current associated with surface charging can affect the interpretation of galvanostatic techniques to separate ionic and electronic current contributions in planar samples with lateral contacts. This is why it is recommended to check the size of capacitances and to measure resistance instead of current in order to avoid gross misinterpretation, as remarked by Zhao *et al.*<sup>81,82</sup>

Abate and coworkers have analyzed the long time behavior of PSCs under cycles of dark and illuminated states (Fig. 14).

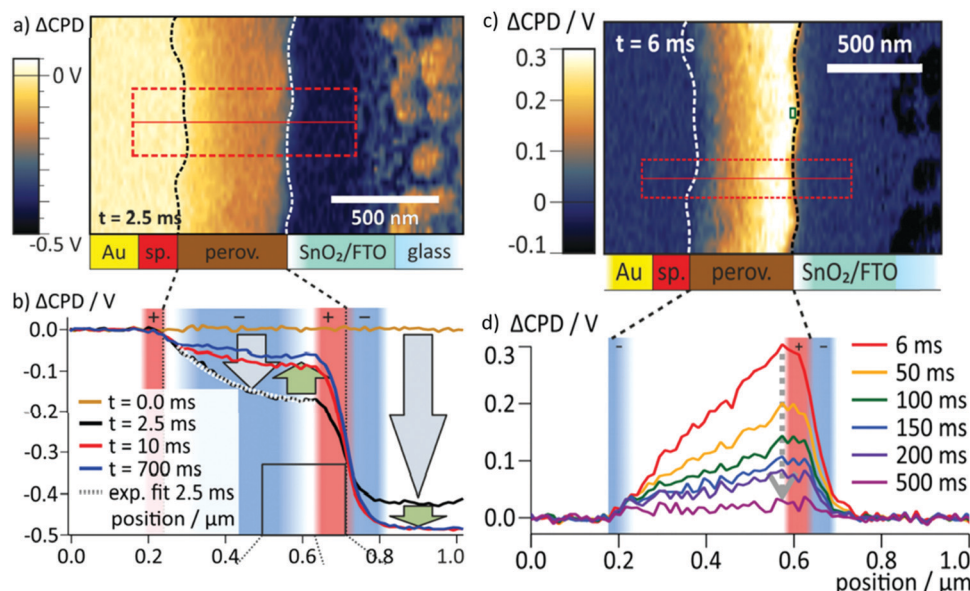


**Fig. 13** Time resolved KPFM results with pulsed illumination. (a)  $\Delta\text{CPD}$  map 2.5 ms after the switching, where a strong potential gradient is present inside the perovskite. (b) Averaged  $\Delta\text{CPD}$  sections from the rectangular area marked in (a). (c) Map of  $\Delta\text{CPD}$  measured 6 ms after switching off the voltage. The interfaces of the perovskite layer are marked with dotted lines. (d) Averaged section graphs obtained from the region indicated by the red box in (c) at different times after the switching. Adapted with permission from ref. 24.

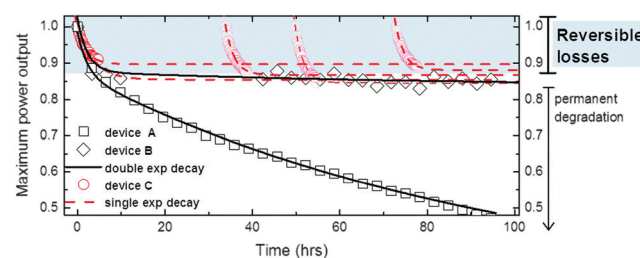


**Fig. 14** Maximum power output tracking for 3 identically prepared perovskite solar cells (device A, B and C) measured under UV-filtered 1 sun equivalent light. Devices were continuously kept at the maximum power point using the standard “perturb and observe” method. Devices A and B were continuously tracked for over 100 hours. Device C was cyclically tracked 4 times for 5 hours and it was left in the dark at open circuit in between the consecutive measurements. Experimental data were fitted to an exponential decay (single or double). Reproduced with permission from ref. 83.

In consonance with the evidence discussed above there is a transient behaviour that occurs between  $10^{-1}$  and  $10^2$  s, which is associated with halide migration and accumulation at the electrode surface. In addition a much longer timescale phenomenon on the order of  $10^3$  s is attributed to cation migration, which eventually leads to contact degradation. This result shows an extreme case in which slow migration does become important to control the kinetics of the PSC, in the case of the  $\text{MA}^+$  cation redistribution,<sup>83</sup> as indicated in Table 2.

In summary, there is a large component of capacitive current often observed but additional kinetic phenomena actuate at the same time and they need to be characterized. These additional phenomena have been described in the very low frequency domain ( $<1$  Hz). We believe it is mandatory to

obtain a full understanding of these effects even for technological reasons. In fact, many claims of “suppressed hysteresis” may denote a successful slowing down of these effects to long times that are imperceptible in the typical range of laboratory measurements, but will nevertheless occur for real operation and practical times as in the example of Fig. 14.

Here we suggest that frequent observation of slow phenomena ( $<1$  Hz) may be interpreted in many cases, beyond the charging-capacitive contribution. The chemical interactions of ions in the perovskite, which introduces a weak bond with the material at the contact, as suggested by Raman analysis for  $\text{MAPbI}_3\text{-TiO}_2$  samples, play an important role.<sup>84</sup> These detailed chemical interactions at interfaces are shown later in Section 9 on the perovskite/contact interface. Generally speaking the chemical interactions are material dependent and they lead to an additional delay in the time to release the ions, being longer than the time for the surface polarization to build-up. In consequence, the surface polarization process introduces not just a capacitive element but also a resistance, and both may be directly related not just by the charging of the double layer but also by surface absorption/reaction processes. In this regard, it has been shown the remarkable result that the time constant in the range of 1 s is independent of the illumination intensity and slightly dependent on the cell thickness as shown in Fig. 15, and hence it is barely affected by the bulk electron concentrations. In order to explain these results, we need to adopt a more general point of view that embraces the dynamic phenomena observed both in solar cells *ca.* 100 nm thick and in much larger samples over 100  $\mu\text{m}$  as described in the pioneering study by Almora, Guerrero and Garcia-Belmonte.<sup>29</sup>

The kinetic process that is characterized in the results of Fig. 15 is clearly related to the slow time constant in the 1 s

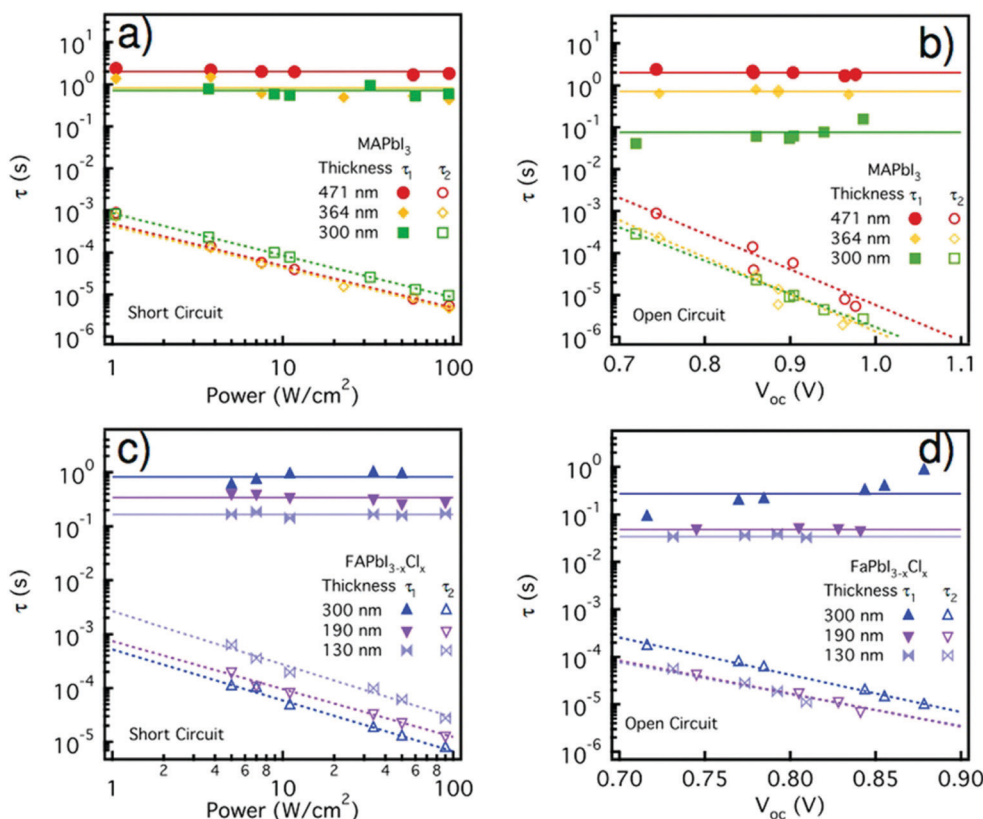


**Fig. 15** Response time calculated from the RC product for the low-frequency arc (solid line) and high-frequency arc (dashed line), respectively. (a) Short-circuit and (b) open-circuit conditions for MAPbI<sub>3</sub>-based planar solar cells and (c) short-circuit and (d) open-circuit conditions for FAPbI<sub>3-x</sub>Cl<sub>x</sub>-based planar solar cells. Reproduced with permission from ref. 28.

domain that has been associated with a predominantly surface process related to ionic interaction with the surface. Nevertheless, the process presents a mixture of interfacial and bulk characteristics. This indicates that charging the double layer involves transport of ions. Therefore the framework of separate time constants for transport and surface complexation suggested in Table 2 needs to be extended. Garcia-Belmonte *et al.* suggested<sup>29</sup> that the ion charging dynamics is composed of an average time for bulk transport in the thickness  $d$  and double layer charging as follows

$$\tau_{\text{char}} = \frac{L_D d}{D} \quad (6)$$

This approach is well established for liquid electrolytes and colloids.<sup>85</sup> In the case that  $L_D \approx 200$  nm, for a distance  $d \approx 400$  nm the  $\tau_{\text{char}}$  in eqn (6) does not differ significantly from bulk diffusion as calculated in Table 2. However, eqn (6) introduces a thickness-dependence of the time constant, as indicated by the solid line in Fig. 16, in agreement with the variations of the time constant noted in Fig. 15. When the layer becomes much larger, in the range of tens of  $\mu\text{m}$ , the effective time constants take values that cannot be explained by bulk diffusion, while the dependence in eqn (6) is in accord with transient current results.<sup>29</sup> When we include the experimental results of Fig. 15 in the graph of Fig. 16, it is obvious that the experimental time constants become much larger than

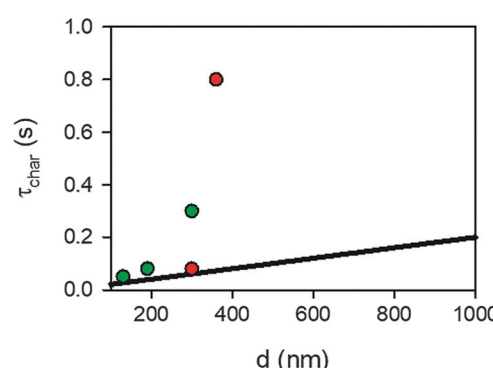


**Fig. 16** Representation of the ionic charging time for diffusion coefficient  $D = 1 \times 10^{-8} \text{ cm}^2 \text{ s}^{-1}$  and Debye length  $L_D = 200 \text{ nm}$  as a function of layer thickness. The points correspond to the data of Fig. 15 for MAPbI<sub>3</sub> (red) and FAPbI<sub>3-x</sub>Cl<sub>x</sub> (green).

expected by simple double layer charging by diffusion as eqn (6). This leads us to the previous conclusion that the  $\tau_{\text{char}}$  time is not explained simply by electrostatics and diffusion. The slow time constant contains these features but, in addition, a significant component of surface binding, related to ionic relaxation suggested in eqn (5), slows down the system, sets the value in the 1 s and longer domain, and eventually produces out-of-phase components leading to inductive behaviour in the frequency domain and a resistance that decreases at low frequency.

Summarizing, we can provide a general perspective of kinetic studies discussed so far in PSCs, based on Fig. 3. Several general circuits have been provided; in most cases there are two basic processes, as in model b, at low and high frequency, which have been normally interpreted in terms of a bulk dielectric capacitance coupled with some resistance and a slow low frequency process fundamentally related to the interface. Nevertheless, sometimes by special experimental procedures three neat processes have been revealed, as in model c and e, which we believe correspond to a decoupling of the separate contacts. In addition it is often observed that the different resistances show correlated variations.

The low frequency process shows in many cases a constant kinetic time, as shown in Fig. 15, independent of current and voltage. Since the constant is the product  $RC$ , the low frequency capacitance and resistance are correlated, which is very frequent in trapping models, and in silicon recombination, for example, in which the reciprocal dependence gives a fairly constant  $\tau$ . However, the additional complexity in PSCs is that the low frequency features have combined properties of electronic and ionic processes, then one can assume that the capacitance is proportional to the carrier densities  $C_s \propto nc$ , while for the resistance, which is inversely proportional to current, one has  $R_1 \propto j^{-1} \propto (nc)^{-1}$ . However, the specific coupling is rather uncertain, and complicates the understanding of the voltage distribution in PSCs (from the separation of Fermi levels at the contacts). This is reflected by the uncertainty of models between series and parallel connection that becomes apparent when we combine the main models in Fig. 3. This limitation of the present understanding may be due to additional complexity that is starting to be revealed, as better and more robust samples become widely available, in comparison with early studies, where many random effects introduced by the experimental itself. For example the hypothesis of a charging process along the bulk is well described in eqn (6), but such a process should correspond to more complicated bulk diffusion with the kinetics indicated in model a of Fig. 3. Models for two or more carriers are not simply composed of series and parallel, so that circuits with two parallel lines or with lumped elements are oversimplifications. Clearly there is a lot of room for careful experimental analysis and interpretation before a more complete picture can be established.

## 7. Mechanism of charging and discharging of the interfaces

There have been intensive efforts to use simulation techniques to predict the properties of the complete device stack as it is widely accepted that surface defects are a source of charge carrier trapping and will affect the extraction properties in photovoltaic devices.<sup>86–88</sup> Comprehensive reviews are available in the literature and detailed analysis is beyond the scope of this work.<sup>89</sup> From the atomistic point of view the different kinetics for charging and discharging are difficult to predict due to the large number of variables to take into account at the interface.

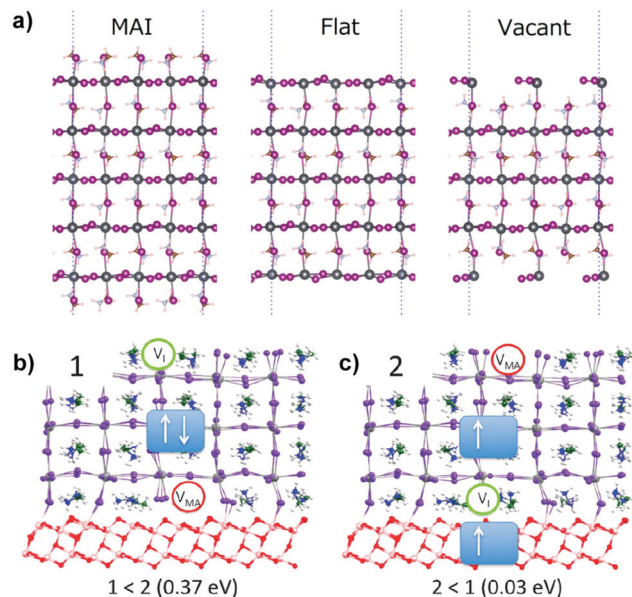


Fig. 17 (a) Examples of perovskite termination. Reproduced with permission from ref. 91. (b) Location of  $V_I$  and  $V_{MA}$  in the ground state with the VB edge localized on the perovskite and (c) in the charge separated state in which one electron has been promoted from the perovskite to the  $TiO_2$ . Reproduced with permission from ref. 92.

Using the 3D periodic boundary condition, the surfaces can be modelled by a slab of a supercell, which consists of atomic layers and a vacuum layer. The interface of the perovskite with the contact is very rich as there can be different terminations; see for example three possible terminations in Fig. 17a. In addition to these terminations the twelve intrinsic point defects (vacancies, interstitials and antisites) present in the bulk of the perovskite would also need to be taken into account at the interface.<sup>90</sup> For example, intrinsic point defects such as vacancies ( $V_I$ ,  $V_{MA}$ ,  $V_{Pb}$ ), interstitials ( $I_i$ ,  $Pb_i$ ) and antisites ( $PbI$ ,  $PbMA$ ) were identified to be formed on each terminated surface (Fig. 17b), and their formation energies have been calculated for I-rich, moderate and Pb-rich conditions.<sup>91</sup> In addition, analysis of the different crystallization indices also leads to different results. Therefore, predicting the actual chemical reactions taking place at the interface is a very difficult task.

De Angelis *et al.* have intensively studied the  $TiO_2/ MAPbI_3$  interfaces using SOC-DFT calculations.<sup>92,93</sup> It was revealed that through interactions of the perovskite with  $TiO_2$  the interface adopts an electronic structure with strong coupling between the  $Ti$  3d and  $Pb$  6p conduction band states and upshifts the  $TiO_2$  conduction band energy.<sup>93</sup> Defects at the interfaces (vacancies  $V_I$  and  $V_{MA}$ ) were studied under working conditions and it was shown that vacancies  $V_I$  diffuse towards the HTL and  $V_{MA}$  towards the ETL side.<sup>92</sup> When compared with the non-defective interface, the outermost valence band states of the perovskite interfere with the band gap of the  $TiO_2$ , while the conduction band states are found inside the conduction states of the oxide. Overall, it was shown that defects at interfaces modify the band alignment, cause the bending of the perovskite bands close to the  $TiO_2$  surface, and create the trap states.<sup>92</sup>

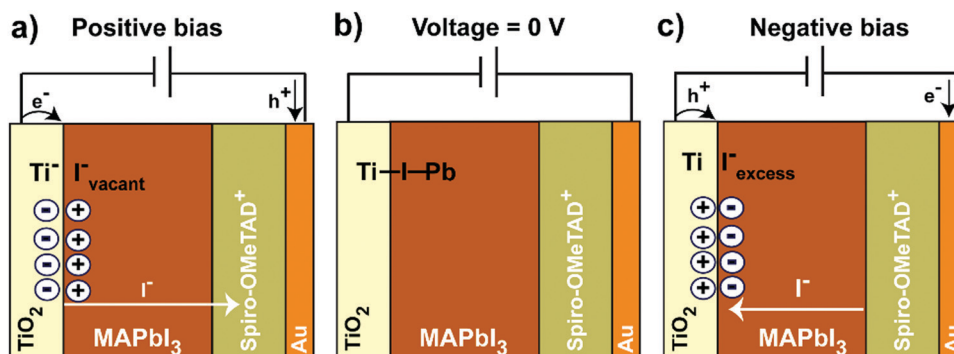


Fig. 18 Diagrams representing iodide migration and the chemical species present at the interfaces that lead to a modification in the capacitance. (a) At positive bias iodine ions are forced to migrate towards the hole selective contact where the chemical reaction with spiro-OMeTAD<sup>+</sup> occurs. An iodine defective layer is formed at the TiO<sub>2</sub>/MAPbI<sub>3</sub> interface. (b) At zero bias the neutral case appears. (c) At negative bias spiro-OMeTAD only partially returns to its oxidized, conductive state. Iodine ions accumulate at the TiO<sub>2</sub>. Reproduced with permission from ref. 84.

Due to the complexity of the system, the precise species formed at the interfaces during charging and discharging are difficult to predict. However, interfacial defects and migrating ions piling up at the contacts will lead to measurable double layer capacitances, both Helmholtz and diffuse layer. The sign and magnitude of the applied bias will modify the capacitance with time due to ion migration and to the chemical reactivity of migrating ions with the external contacts as it will be discussed below.<sup>84</sup> Fig. 18 shows a simplistic view that highlights the direction of migration for only one ion as detected by capacitive current measurements in the dark. Due to the rich chemistry of iodine and to the presence of oxidative conditions, once ions reach the external contacts these can react with the contact material, as described below, further modifying the capacitance. The kinetics of this type of reactions will be slower than that of ion migration since the availability of ions will be a requirement for the chemical reaction to take place. Therefore, chemical reactivity will be observed at long timescales (Fig. 1) and low frequencies during impedance measurements.

## 8. Ferroelectric effects

There have been over the years different speculations on the influence of a ferroelectric property on the PV behaviour of perovskite solar cells. Obtaining a permanent, switchable polarization in electrical insulators is relatively easy to determine by electrical methods. However, in the case of a metal halide perovskite semiconductor with contacts (necessary for PV application), there are intrinsic leakage currents and an ionic polarization component so the true polar domain orientation is rather challenging to confirm.<sup>94,95</sup> Recently the observation of ferroelectric polarization in metal halide perovskites has been reported by different methods.<sup>95–98</sup> However, it is rather unclear that such a property has any significance for the PV properties. The use of ferroelectric materials in solar energy conversion has been reviewed elsewhere.<sup>99</sup> The application of an electrically polarized material as a solar cell aims to benefit from charge separation by the electrical field. Most of the materials reported in the literature are wide bandgap extreme

insulators,<sup>99</sup> they provide a tiny photocurrent, the polarization is always affected by a depolarising field, and the PV mechanism is rather uncertain in most cases: since electrical contacts normally shield the internal field, most observed characteristics are believed to be associated with the contact properties. For example migration of defects can modify the contact Schottky barriers by poling and produce a switchable characteristic of the photocurrent.<sup>100,101</sup> In addition, charge separation is not a real issue in the metal halide perovskites that enjoy excellent semiconductor properties. Therefore the role of ferroelectrics in PV behaviour should be rather minor.

Another potentially useful pathway to exploit the ferroelectric property is to build active thin switchable layers that improve the operation of contacts, or facilitate some type of memory device. In principle one can change the built-in voltage according to the state of the surface ferroelectric layer.<sup>102</sup> However, for low conductivity or depletion in the semiconductor the surface charge in the thin ferroelectric layer cannot be cancelled at the active material side. This situation leads to a large uncompensated field in the ferroelectric layer that will remove the polarization charge.<sup>103</sup> Recently this approach was realized for obtaining a switchable response in perovskite solar cells,<sup>104</sup> but issues of charge compensation and ionic polarization make the interpretation of results rather difficult.

## 9. Perovskite/contact interface: chemical, structural and energetic properties

So far we have focused on the physical implications of ionic migration on material and device performance. In the following part, we consider the main types of chemical interactions at the perovskite/contact interface. Specifically we cover some morphological and chemical aspects that relate to the kinetic charge distribution and thus require some attention to design a PSC stack with increased stability and without hysteresis.

It is well known that the properties of interfaces are a dominant aspect of electronic devices such as solar cells.

Therefore, lots of efforts have been devoted to develop the contacts in order to obtain high quality interfaces with desirable properties for high performance devices. The variety of contacts used as the ETL and HTL in PSCs is almost endless and several recent reviews cover these aspects in detail.<sup>3–5</sup> In general, ETLs include metal oxides (*i.e.* TiO<sub>2</sub>, SnO<sub>2</sub> or ZnO) or organic molecules (*i.e.* fullerenes). Similarly, materials used as HTLs also embrace metal oxides (*i.e.* NiO<sub>x</sub>), CuSCN, CuI and organic compounds such as spiro-OMeTAD, PEDOT:PSS or conductive carbon.<sup>5,105</sup> We anticipate that chemically robust contacts are required to withstand the highly reactive perovskite interface, enabling efficient extraction of carriers. In general, electron/hole accumulation at the interfaces in the presence of migrating ions may lead to their degradation.

### Morphology of contacts

Apart from all the chemical interactions, the roughness of the FTO substrate can also affect the hysteresis of PSCs as reported by Cojocaru *et al.*<sup>106</sup> Compared to the FTO with higher roughness, better device efficiency and relatively smaller hysteresis were obtained with the FTO with a flat surface. Because of the different roughness of the FTO contact, the effect of surface treatment by TiCl<sub>4</sub> solution differs significantly, where TiCl<sub>4</sub> treatment showed effectiveness on a rough FTO surface compared to a flat one. This is ascribed to the different surface contact degree with the perovskite, as the flat FTO surface has better contact with the perovskite, which ultimately leads to homogeneous accumulation of carriers at the interfaces.<sup>106</sup> Nanometer-scale *in situ* current–voltage measurements used to detect the current flow at the interface of TiO<sub>2</sub>/perovskite showed a tunneling current at the TiO<sub>2</sub>/perovskite interface when TiO<sub>2</sub> with a rough surface was used, while such a leak current was not observed with the TiO<sub>2</sub> with a smooth surface (Fig. 19). The tunneling current was believed to be caused by the local-heavy doping due to the electrostatic dipole at a rough TiO<sub>2</sub>/perovskite interface, which triggers a chain reaction of charge accumulation, in turn causing more severe hysteresis in the *j*–*V* plot.<sup>107</sup>

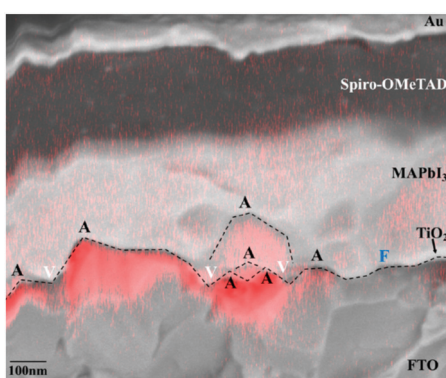


Fig. 19 EBIC results showing the electron density map at apexes (black A), valleys (white V) and the flat interface (blue F) on a cross-sectional SEM image of a PSC. Reproduced with permission from ref. 107.

### ITO/PEDOT:PSS/Perovskite/PCBM/Metal

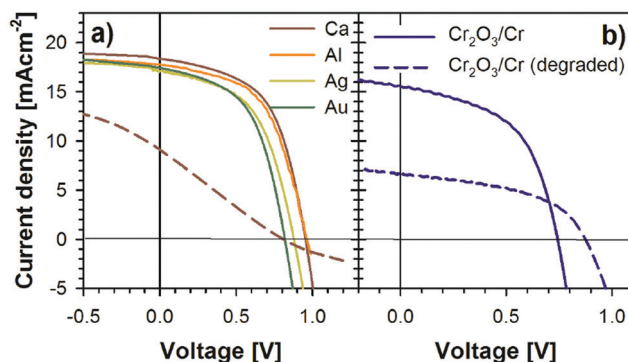


Fig. 20 Current density–voltage curves of devices fabricated with different metal contacts measured at 1 sun light illumination. (a) Metals providing S-shape curves after degradation. (b) The contact containing Cr<sub>2</sub>O<sub>3</sub>/Cr does not show an S-shape after degradation. Degraded devices are shown as broken lines. Reproduced with permission from ref. 108.

### Metal/perovskite contacts

There are several metals that have been used as the current collector layer in the device configuration, such as Ca, Al, Ag, Au or Cr (Fig. 20).<sup>108</sup> These contacts formed between the metal and perovskite provide simple devices for mechanistic study. Perovskites have been proved to oxidize the metals, generating their corresponding halides (*i.e.* CaI<sub>2</sub>, AlI<sub>3</sub> or AgI). For example, oxidation of Ag to form AgI has been widely studied by a range of techniques like XRD or XPS.<sup>109</sup>

A mechanism such as that shown in Fig. 21 has been proposed in the presence of ambient water, in which water reacts with the perovskite layer leading to formation of PbI<sub>2</sub> and subsequent iodine migration and surface diffusion form AgI. Even noble metals such as Au also lead to corrosion at the interface level under oxidative stress.<sup>110</sup> When used as a current collector with a buffer layer (*i.e.* perovskite/ETL/metal), a small area or pinhole not covered by the buffer layer is sufficient to lead to corrosion of the metal. In addition, due to the soft nature of the perovskite, metal diffusion through the perovskite has also been observed by analytical techniques like TOF-SIMMS.<sup>111</sup>

A thin buffer layer of chromium (Cr/Cr<sub>2</sub>O<sub>3</sub>) has proved to be very useful for stopping corrosion of the current collector.<sup>108,112</sup> Tisdale *et al.* investigated the contact formed by MAPbBr<sub>3</sub> single crystals and metal Cr or Au. They have found that the contact between the perovskite and Cr is ohmic while when using Au to replace Cr, the contact property is switched to non-ohmic. Because of the different contact property, the perovskite/Cr showed a higher interfacial charge transfer resistance ( $R_{ct}$ ) of  $1.79 \times 10^9 \Omega$  compared to perovskite/Au ( $R_{ct} = 1.32 \times 10^7 \Omega$ ).<sup>113</sup> This is in contrast to the general understanding that the contact between the perovskite and Au is ohmic.<sup>114</sup> Clearly more work is needed to understand the contact property of perovskite/contact for current collector materials such as metal, carbon *etc.*, which is particularly important for HTL-free PSCs. Since Cr is very stable in the presence of iodine, it thus could be a promising electrical contact for PSCs to be considered in the future. The study on a

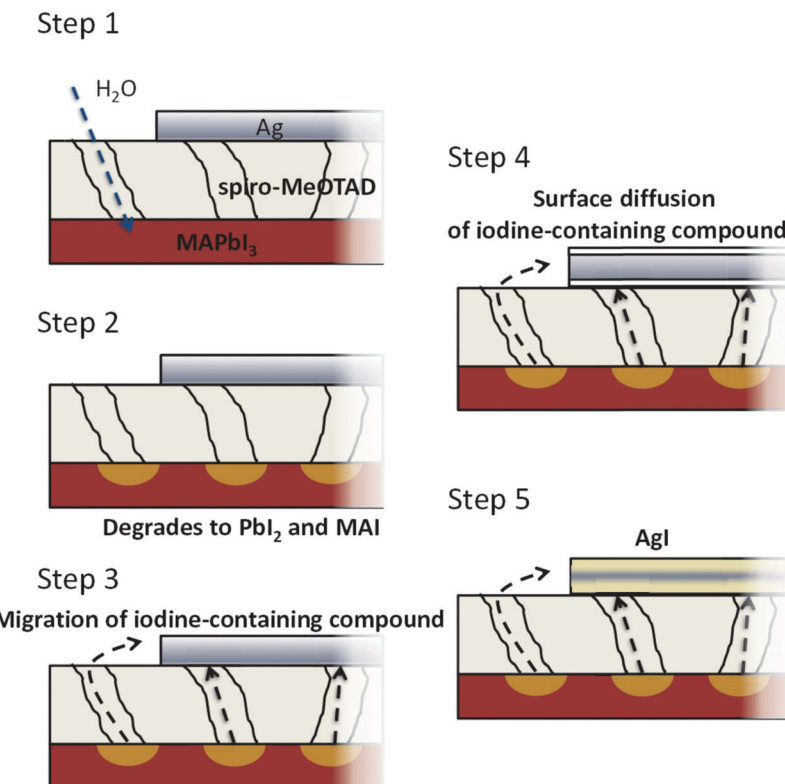


Fig. 21 Proposed  $AgI$  formation mechanism in the presence of ambient water. Reproduced with permission from ref. 109.

$MAPbBr_3$  single crystal in direct contact with ITO (or  $TiO_2$ ) and a Au based electrical contact (device structure: ITO/perovskite/Au or FTO/ $TiO_2$ /perovskite/Au) shows that, compared to a  $TiO_2$  based ETL, the ITO based PSC showed an even higher  $J_{sc}$  (7.4 mA cm<sup>-2</sup> vs. 7.0 mA cm<sup>-2</sup>), but a smaller  $V_{oc}$  (1.25 V vs. 1.36 V) and FF (0.59 vs. 0.69) in the reverse scan. In the forward scan, the ITO based device showed much poorer performance, leading to very large hysteresis compared to the  $TiO_2$  counterpart. The poor charge extraction at the interface of ITO/perovskite was blamed for this phenomenon.

#### ETL/perovskite interface and reactivity

$TiO_2$  is one of the most widely used electron transport material in PSCs, and some of its modifications were already commented on in Section 5. Research has shown that  $TiO_2$  is actually not an ideal ETL material in terms of energetic level matching with the adjacent perovskite and stability under UV-light. Mesoporous  $TiO_2$  was reported to have a higher conduction band edge ( $E_{cb}$ ) relative to that of perovskite  $MAPbI_3$ , causing inefficient interfacial charge injection. The periodic table has been scrutinized with several types of dopants for the  $TiO_2$  layer. The general aim has been to improve the conductivity whilst not modifying greatly the band edges of  $TiO_2$ . The overall effect has been to improve the extraction properties of the contact and reduce recombination pathways. For example,  $TiO_2$  has been doped with a wide variety of ions such as Li,<sup>115</sup> Ru,<sup>116</sup> Fe,<sup>117</sup> Co,<sup>118</sup> Y,<sup>119</sup> Cd,<sup>120</sup> La,<sup>121</sup> Sm,<sup>122</sup> Nb,<sup>123</sup> Er,<sup>124</sup> Ta,<sup>125</sup> Pt,<sup>126</sup> Zn,<sup>127</sup> Ga,<sup>128</sup> In,<sup>129</sup> or Sn.<sup>130</sup> Doping  $TiO_2$  with an alkaline cation such

as lithium has been reported to improve its electronic properties such as a reduced trap density, thus enhancing the dynamics of interfacial charge transfer.<sup>131</sup> Similarly, introduction of potassium cations ( $K^+$ ) into the perovskite film has also been demonstrated as an effective way to eliminate  $j$ - $V$  hysteresis of PSCs. The location of  $K^+$  in the perovskite crystal lattice is still under debate, but concrete experimental results show the conduction band edge of the perovskite is shifted downward, leading to a more favourable energy alignment with  $SnO_2$  for charge transfer.<sup>132</sup> Surface treatment of  $TiO_2$  film with fluorine ( $CF_4$ )-based plasma was found to enhance the interface adhesion between the perovskite and the  $TiO_2$ .<sup>133</sup> The fluorine doped  $TiO_2$  was also found to offer a more favourable energy alignment with the adjacent perovskite material. Consequently, a dramatically improved device efficiency and reduced hysteresis in the  $j$ - $V$  plot were achieved.

The metal oxide  $SnO_2$  has a lower conduction band and larger band gap (3.5–3.6 eV) than  $TiO_2$ , therefore it is normally considered that the charge transfer at  $SnO_2$ /perovskite is more efficient compared to  $TiO_2$ /perovskite. The pioneering work of Correa-Baena *et al.*<sup>134</sup> demonstrated the excellent properties of  $SnO_2$  for planar contacts in PSCs in comparison to planar  $TiO_2$ , hence tin oxide has henceforth become a popular ETL in planar cells. The subsequent study by impedance spectroscopy of the same cells<sup>31</sup> revealed an enormous difference of dynamic properties and marked the standard models for IS in the literature, which is presented here in Fig. 3c. The material properties of the interface of  $SnO_x$  with halide perovskites were

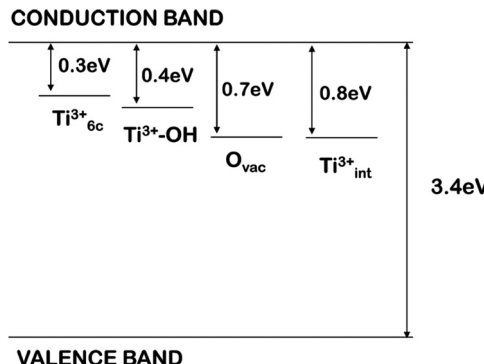
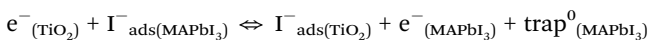


**Fig. 22** Schematic representation of the defect energy levels in the band gap of bulk anatase  $\text{TiO}_2$  as derived from B3LYP calculations for the following  $\text{Ti}_{3+}$  species: (1) 6-fold-coordinated  $\text{Ti}_{6\text{c}3+}$ ; (2)  $\text{Ti}_{6\text{c}3+}\text{-OH}$  species; (3)  $\text{Ti}_{5\text{c}3+}$  species associated with oxygen vacancies; and (4) interstitial  $\text{Ti}_{5\text{c}3+}$  species. Reproduced with permission from ref. 137.

characterized by Riedl, Olthof and coworkers,<sup>135</sup> who showed the spontaneous formation of a  $\text{PbI}_2$  interfacial layer. An ETL based on a bilayer of compact crystalline- $\text{TiO}_2$ /amorphous- $\text{SnO}_2$  was reported to enhance the charge extraction of PSCs and reduce hysteresis at the same time as a result of improved interface band alignment with triple cation ( $\text{Cs}_{0.05}\text{MA}_{0.15}\text{FA}_{0.85}\text{Pb}(\text{I}_{0.85}\text{Br}_{0.15})_3$ ).<sup>136</sup>

The chemistry at the interfaces of PSCs is responsible for many of the phenomena observed in the device. Limited research has indicated chemical reactions occurring at the interface of  $\text{TiO}_2$ /perovskite and perovskite/HTL. The Raman spectrum of a symmetrical cell of FTO/ $\text{TiO}_2$ /perovskite/ $\text{TiO}_2$ /FTO has confirmed the formation of Ti–I–Pb bonds, which are able to accommodate accumulated charge, leading to a capacitive current.<sup>84</sup> The highly reversible current–voltage plot indicates that the process associated with charge storage of Ti–I–Pb is reversible. Generation of this type of chemical bonds is compatible with reactivity with  $\text{Ti}^{3+}$  defects present in the  $\text{TiO}_2$  layer (Fig. 22). Prevalent  $\text{Ti}^{3+}$  defects are present in  $\text{TiO}_2$  in the tail of the conduction band and these defects are known to control the electronic response of some PV devices.<sup>137</sup> The dynamic response of the interface in light soaking experiments in organic PVs clearly highlights that these defects are highly reactive and can interact with molecular oxygen.<sup>138,139</sup>

The reversible chemical reactions at  $\text{TiO}_2$ /perovskite interfaces have also been proposed based on indirect evidence of a reversible response showing chemical adsorption/desorption of  $\text{TiO}_2$ /iodine gas and  $\text{MAPbI}_3$ /iodine gas which occurs on the time scale of seconds to minutes.<sup>140</sup> If the same reaction applies to the  $\text{TiO}_2$ /perovskite solid–solid interface, the proposed reversible reaction is:



These charge transfer reactions explain the large reversible capacitance observed with PSCs. Clearly the different surface defect property of  $\text{TiO}_2$  can affect its reaction with  $\text{I}^-$  of  $\text{MAPbI}_3$ , thus the device performance and hysteresis. Therefore, apart from increasing the conductivity of the ETL, other aspects like

avoiding the reactivity of migrating ions with defects are required in order to control the  $j$ – $V$  response and stability.

Different methods have been reported to passivate the surface defects of  $\text{TiO}_2$  by using small molecules such as PCBA, PCB and  $\text{C}_{60}$ .<sup>141</sup> The surface modifier did not lead to a change of the morphology, crystallinity and bulk defect density of the perovskite layer that was deposited above the  $\text{TiO}_2$  layer coated with the modifier. However, more efficient charge extraction and recombination dynamics were observed at the interface of perovskite/ $\text{TiO}_2\text{-C}_{60}$  compared to bare  $\text{TiO}_2$ , leading to much better performance and reduced hysteresis. An attempt to eliminate the current–voltage hysteresis of PSCs through tuning the interfacial chemical composition of perovskite/ETL by using a self-assembled monolayer (SAM) was also reported.<sup>142</sup> It was found that the PSCs had a thin layer of a several-angstrom thick MAI-rich (Pb-poor) interface between the perovskite and the metal oxide, which caused formation of a large capacitance and thus  $j$ – $V$  hysteresis. By applying a self-assembled monolayer consisting of a 6-octyl phosphonic acid ( $\text{C}_6\text{-PA}$ )– $\text{C}_{60}$ – $\text{C}_6\text{-PA}$  mixture above the  $\text{TiO}_2$  based ETL, the interfacial composition is switched from Pb-poor to Pb-rich while the property of the perovskite bulk was not affected. The chemical reactivity with  $\text{TiO}_2$  is avoided in the SAM modified PSCs. This is explained by the capability of the Pb-rich interface to compensate the ionic accumulated charge, therefore suppressing the net charge at the interface and the capacitance, leading to elimination of the  $j$ – $V$  hysteresis.

The important influence of interfacial chemical interactions on both the performance and hysteresis of PSCs is also shown by Zou *et al.*<sup>143</sup> Using a series of SAMs containing different functional groups, they have found that the chemical interaction between the SAM and perovskite dominates the device performance instead of the energy position.<sup>144</sup> A polymer fullerene film (PMMA–PCBM) was found to effectively passivate defects at or near to the perovskite/ $\text{TiO}_2$  interface, thus dramatically suppressing interfacial recombination. The interfacial passivation layer not only enhanced the  $V_{oc}$  of the cell up to 80 mV, but also removed the  $j$ – $V$  hysteresis.<sup>145</sup> Patel *et al.* have found that different interface contacts can affect the morphology of the perovskite layers, which in turn affected the device performance and hysteresis. The study of vapor-deposited  $\text{MAPbI}_3$  on four different ETL contact layers including compact  $\text{TiO}_2$ ,  $\text{C}_{60}$ , compact  $\text{TiO}_2$ /PCBM and poly-TPD showed regions of amorphous  $\text{MAPbI}_3$  close to the  $\text{TiO}_2$  layer, which was attributed to the lattice mismatch between them. The amorphous  $\text{MAPbI}_3$  at the interface led to poor charge collection and severe charge recombination, thus device hysteresis occurs via the electrical capacitive effect.<sup>146</sup> This finding tells us that the morphology change of the perovskite in the presence of different contacts should not be ignored when studying the hysteresis of PSCs.

Besides surface passivation, the interface property of ETL/perovskite can also be modified by tailoring the composition of the ETL. Recent work has shown that the  $j$ – $V$  hysteresis of PSCs using  $\text{SnO}_2$  as the ETL could be related to the density of oxygen vacancies in the  $\text{SnO}_x$  film. By increasing the density of oxygen

vacancies of the  $\text{SnO}_2$  thin film made by sputtering deposition through increasing the annealing temperature, the efficiency of PSCs was improved owing to the significantly enhanced  $V_{\text{oc}}$ . At the same time, the  $j$ - $V$  hysteresis was substantially reduced.<sup>147</sup> An inorganic salt such as KCl was used to passivate the interface defects of  $\text{SnO}_2$ , which leads to a fast photocurrent response and an elongated lifetime. As a result, the efficiency of the device was enhanced while the hysteresis was suppressed.<sup>143</sup>

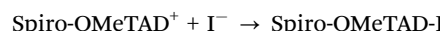
### HTL/perovskite interface and reactivity

Similar to the ETL, the kinetics in the reactivity at the HTL/perovskite interface can determine the electrical response and stability of the device.<sup>105</sup> The nanoporous carbon electrodes developed by Han and coworkers are one of the most successful HTLs with the first report to show promising device stability exceeding 1000 h under full sun illumination.<sup>148</sup> The results indicated that the HTL material was compatible with the oxidative conditions generated in the perovskite layer and interface. In this process a stack containing mesoporous layers of different materials is filled with the perovskite precursor solution. Once the solvent is evaporated the perovskite forms inside the pores, whilst the interfacial chemistry will depend very much on the preparation method of the carbon ink. Hysteresis has been suppressed by controlling the thickness of the  $\text{TiO}_2$  underlayer. It indicates that the carbon must have a small concentration of functional groups which can chemically interact with the migrating ions.<sup>37</sup>

Alternatively, if an organic HTL is deposited by solution processes on the top of the perovskite a thick layer of hundreds of nanometers will be required to avoid the exposure of the perovskite to the metal based current collector electrode. Due to the relatively low conductivity of the current organic HTLs the use of additives is usually needed, which, however, gives rise to some issues. On the one hand, lithium derivatives are used to stabilize oxidized species generated during light soaking of the spiro-OMeTAD, which increases the conductivity.<sup>149,150</sup> On the other hand, bases like *tert*-butyl pyridine (tBP) as an additive are usually used in spiro-OMeTAD to tune the electronic properties of the layer. Unfortunately, both type of additives will interact with the perovskite, with  $\text{Li}^+$  being able to migrate through the perovskite and the basic pyridine coordinating to the lead atoms of the perovskite.<sup>23,151</sup> For example, using time of flight secondary-ion mass spectroscopy (TOF-SIMS), a technique able to probe the chemical reactions at the interfaces of PSCs, phase segregation and migration of extrinsic small cations like  $\text{Li}^+$  were confirmed.<sup>152</sup> A gradient of A-site inorganic cations is observed in the perovskite film, where it is rich at the back contact.<sup>153</sup> Meanwhile, degradation of the perovskite due to the impact of tBP has been reported in the literature.<sup>154</sup> It is believed that the perovskite can react with tBP, resulting in formation of the  $\text{PbI}_2$ -tBP intermediate and MAI product.

Very importantly, migrating ions in the perovskite layer will be able to react or diffuse into the HTL, leading to different responses. For example, the oxidized form of the widely used organic hole transport molecule spiro-OMeTAD will lead to formation of the neutral iodine derivative spiro-OMeTAD-I.<sup>84</sup> Of course, other side products will be generated, which could in

turn have their own impact. The reaction would be irreversible, therefore causing permanent change/damage to the device performance including the efficiency and stability.<sup>147</sup>



Stabilization of the cation leads to devices with increased stability in comparison with spiro-OMeTAD as shown by Schloemer *et al.*<sup>155</sup> However, degradation is still severe under operation conditions. To avoid this type of reactivity, dopant-free HTLs have been designed by different groups. Brabec *et al.* have designed some conjugated polymers and have shown that the PDCBT derivative is a successful candidate able to withstand oxidative conditions generated by  $\text{I}^-/\text{I}_3^-$  (Fig. 25).<sup>62,156</sup>

In addition, the use of metal oxides between the organic HTL and the current collector has been adopted with the aim to act as a physical barrier to stop ambient water diffusing into the device and the migration of iodine to the current collector.<sup>156,157</sup> With this purpose  $\text{MoO}_x$  and  $\text{Ta-WO}_x$  have been used successfully. The reactivity of iodine with the current collector is reduced by having this additional layer as can be observed in Fig. 23 and the stability under ambient conditions is enhanced.<sup>157</sup> However, an organic layer is needed at the interface between the perovskite and the metal oxide as otherwise there is a chemical reaction that forms  $\text{MoO}_2$ , which reduces the ability of the system to extract charge.<sup>158</sup>

By careful alignment of the conduction band of the perovskite and the HOMO level of the hole extraction layer, charge accumulation at the interfaces is avoided, thus reducing hysteresis and increasing the stability of the whole stack dramatically.<sup>35</sup> In the design of the HTL it is important to tune the energy levels to withstand oxidizing agents like  $\text{I}_2$  that can be generated *in situ* by the migrating iodide ions and a significant presence of holes (Fig. 24).

### Identification of chemical reactions in complete PSCs during their lifetime

Perovskite solar cells are notorious for their unsatisfactory stability due to the ease of degradation in the presence of water, oxygen, UV-light, external electrical bias, high temperature *etc.*<sup>159</sup> In this final section, we would like to highlight that during the lifetime of PSCs several physical processes and chemical reactions will be occurring simultaneously, each on their own timescale. Therefore, direct detection of the reaction product is a big challenge in practice and advanced analytical techniques are required to envisage the whole picture of the degradation processes. One representative example is provided by Sultana *et al.* who investigated degradation at the interface level under ambient conditions with the design configuration ITO/ZnO/MAPbI<sub>3</sub>/spiro-OMeTAD/Ag.<sup>160</sup> Identification of the degradation products from the reaction at the interfaces of PSCs has been achieved using laser desorption/ionization mass spectroscopy (LDI-MS). These authors found that after two weeks, the perovskite decomposed to  $\text{PbI}_2$ . Meanwhile other products such as  $\text{ZnI}_2$ ,  $\text{PbO}$  and  $\text{AgI}$  were also detected in the stability testing process. It is believed that the formation of  $\text{PbO}$  is caused by oxygen-mediated photo-reduction (eqn (7a)–(7c)). Besides  $\text{PbO}$ , another product in the degradation reaction is iodine ( $\text{I}_2$ ).

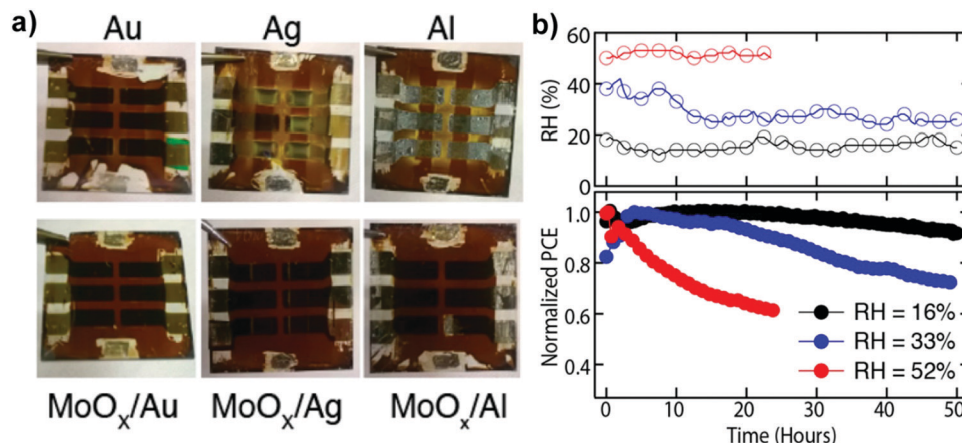


Fig. 23 (a) Optical images of devices containing different current collectors after 24 h of constant operation under ambient conditions. (b) Normalized PCE of similarly fabricated cells measured in three different RH conditions. All of the devices had the same electrode configuration of 15 nm of MoO<sub>x</sub>/200 nm of Al. Reproduced with permission from ref. 157.

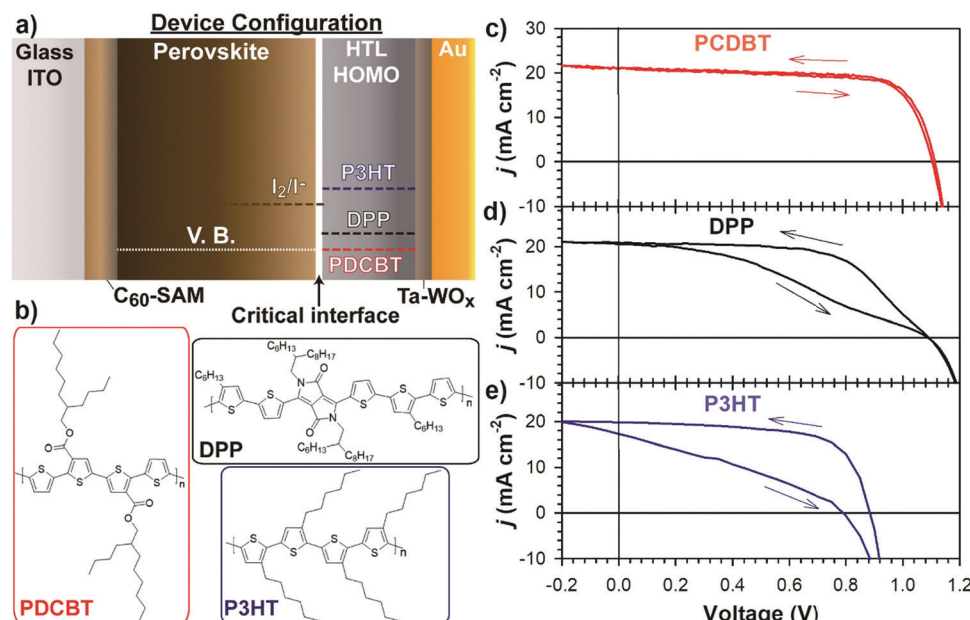
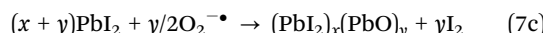
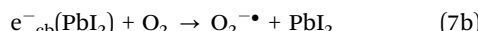
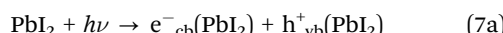


Fig. 24 (a) Device configuration where the HTL is the only parameter that has been modified. (b) Chemical structure of different HTLs. (c–e) *j*–*V* curves of PSCs with different HTLs. Reproduced with permission from ref. 35.

The formation of MA, HI and PbI<sub>2</sub> is a consequence of degradation of MAPbI<sub>3</sub> caused by water and oxygen (eqn (7e) and (7f)).<sup>87,160</sup>



Diffusion of HI to the ZnO based ETL in the cell architecture leads to the formation of ZnI<sub>2</sub> ( $\text{ZnO} + \text{HI} \rightarrow \text{ZnI}_2 + \text{H}_2\text{O}$ ).

Meanwhile ZnI<sub>2</sub> can also be formed by reaction with MAI, which is the product of the decomposition of MAPbI<sub>3</sub>. Due to the presence of high concentrations of electrons and holes and the reactivity of some of the reagents present in devices (*i.e.* oxygen, iodide), the redox chemistry also needs to be considered. Indeed, the oxidant iodine (I<sub>2</sub>) has been reported to form in the device. It is responsible for formation of AgI ( $2\text{Ag} + \text{I}_2 = 2\text{AgI}$ ). The redox chemistry can be predicted by taking into account the position of the energy levels as shown in Fig. 25a. For example, Ag with a band full of electrons at  $\sim -4.7$  eV will favour the redox reaction with the oxidant system I<sup>-</sup>/I<sub>2</sub> at  $\sim -5.0$  eV. Similarly, reactivity with the oxidant iodine can also be a problem with the HTL. The reactivity of I<sup>-</sup>/I<sub>3</sub><sup>-</sup> with a series of three different HTLs is monitored by the color change of the HTL layers (Fig. 25b and c).

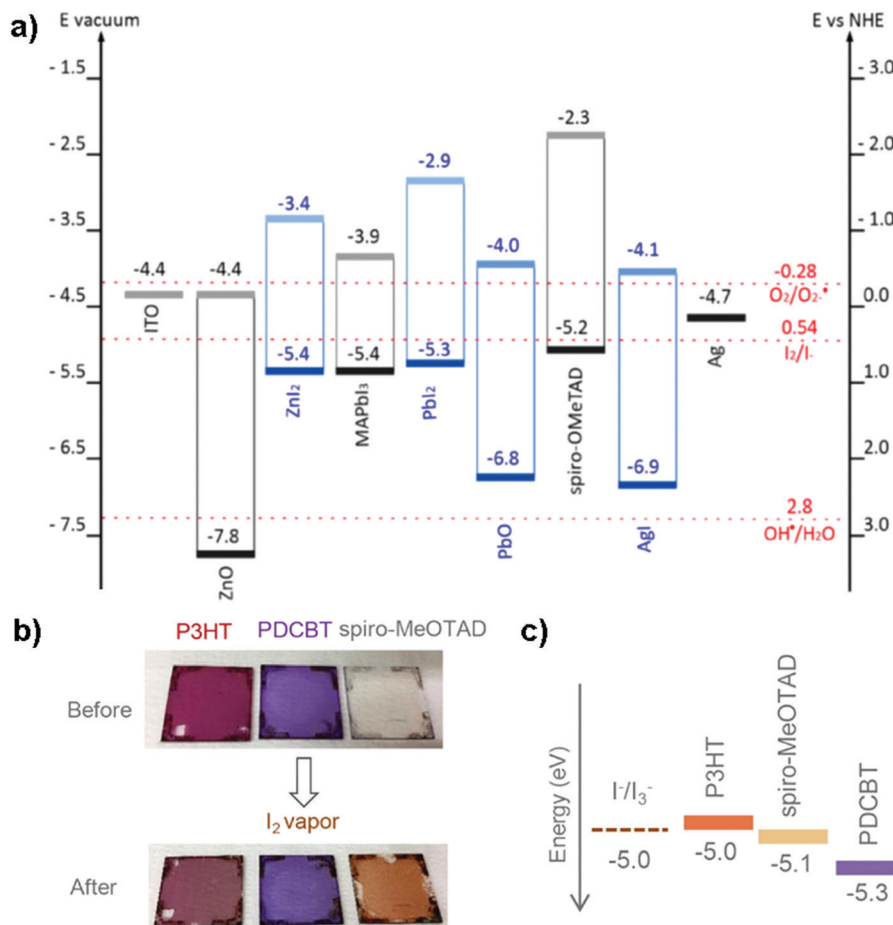


Fig. 25 (a) Energy level diagram of the material employed (black) and formed (blue) in the studied PSCs as well as the potential of side redox reactions (red) occurring in the PSCs. Reproduced with permission from ref. 160. (b and c) Redox reactivity of different HTLs with I<sup>-</sup>/I<sub>3</sub><sup>-</sup>. Reproduced with permission from ref. 156.

Overall, understanding all the chemical processes occurring in a complete solar cell is a very challenging task. Not only acid–base chemistry needs to be considered in relation to the migrating ions but also redox and radical chemistry. Comprehensive analysis of the product as a result of the interfacial reactions of a complete PSC cell with different contacts can provide important information on the cause of the device stability and *j-V* hysteresis. To date, such research is very limited. In the future, more work is clearly needed in this direction, in particular understanding the interface reactions of carbon based HTM-free perovskites may provide new insights into their working mechanism.

## 10. Conclusion and outlook

We have summarized the evidence for surface charge and discharge phenomena at the contacts of perovskite solar cells. Surface charge and discharge processes seem to follow markedly different kinetics, as in asymmetric trapping–detrapping associated with surface binding effects. On the one hand, the supply of ions from the bulk of the perovskite material is fast under the

effect of an electrical field or light. Ions will be transported to the contacts on the timescale of milliseconds for a typical semiconductor thickness of 100–200 nm. These ions will interact physically or chemically with the contacts, generating an electrostatic potential. Depending on the nature of these interactions the release of the ions will be favoured (*i.e.* PCBM) or impeded (*i.e.* metal oxides). Ions present at the interface are detected by impedance spectroscopy as a very large surface capacitance that appears in the very low frequency domain. This capacitance clearly correlates with the observed hysteresis during the *j-V* measurements. There are different approaches to reduce this charged surface such as the use of interfacial layers at the perovskite/extraction layer or the use of additives in the perovskite formulation. In general, the use of additives in the perovskite composition may show incorporation into the crystal lattice but the dynamic electrical properties seem to be related to the interfaces.

## Conflicts of interest

There are no conflicts to declare.

## Acknowledgements

We are thankful for financial support from the Australian Research Council (ARC) through a discovery project (ARC DP 190102252) and Ministerio de Ciencia, Innovación y Universidades of Spain under project (MAT2016-76892-C3-1-R). A. G. would like to thank MICINN for a Ramón y Cajal Fellowship (RYC-201416809). Universitat Jaume I is also acknowledged for financial support (UJI-B2017-32).

## References

- D. Weber, *Z. Naturforsch., B: Anorg. Chem., Org. Chem.*, 1978, **33**, 1443–1445.
- A. Kojima, K. Teshima, Y. Shirai and T. Miyasaka, *J. Am. Chem. Soc.*, 2009, **131**, 6050–6051.
- A. Fakharuddin, L. Schmidt-Mende, G. Garcia-Belmonte, R. Jose and I. Mora-Sero, *Adv. Energy Mater.*, 2017, **7**, 1700623.
- B. Roose, Q. Wang and A. Abate, *Adv. Energy Mater.*, 2019, **9**, 1803140.
- W. Zhou, Z. Wen and P. Gao, *Adv. Energy Mater.*, 2018, **8**, 1702512.
- P. Schulz, *ACS Energy Lett.*, 2018, **3**, 1287–1293.
- J. M. Azpiroz, E. Mosconi, J. Bisquert and F. De Angelis, *Energy Environ. Sci.*, 2015, **8**, 2118–2127.
- T.-Y. Yang, G. Gregori, N. Pellet, M. Grätzel and J. Maier, *Angew. Chem., Int. Ed.*, 2015, **54**, 7905–7910.
- I. Mora-Seró, G. Garcia-Belmonte, P. P. Boix, M. A. Vázquez and J. Bisquert, *Energy Environ. Sci.*, 2009, **2**, 678–686.
- T. Kirchartz and U. Rau, in *Advanced Characterization Techniques for Thin Film Solar Cells*, ed. D. Abou-Ras, T. Kirchartz and U. Rau, Wiley, Berlin, 2011, p. 14.
- Q. Wang, S. Ito, M. Grätzel, F. Fabregat-Santiago, I. Mora-Seró, J. Bisquert, T. Bessho and H. Imai, *J. Phys. Chem. B*, 2006, **110**, 19406–19411.
- F. Fabregat-Santiago, J. Bisquert, E. Palomares, L. Otero, D. Kuang, S. M. Zakeeruddin and M. Grätzel, *J. Phys. Chem. C*, 2007, **111**, 6550–6560.
- H. Wang and L. M. Peter, *J. Phys. Chem. C*, 2009, **113**, 18125–18133.
- H. J. Snaith, A. Abate, J. M. Ball, G. E. Eperon, T. Leijtens, N. K. Noel, S. D. Stranks, J. T.-W. Wang, K. Wojciechowski and W. Zhang, *J. Phys. Chem. Lett.*, 2014, **5**, 1511–1515.
- H.-S. Kim and N.-G. Park, *J. Phys. Chem. Lett.*, 2014, **5**, 2927–2934.
- R. S. Sanchez, V. Gonzalez-Pedro, J.-W. Lee, N.-G. Park, Y. S. Kang, I. Mora-Sero and J. Bisquert, *J. Phys. Chem. Lett.*, 2014, **5**, 2357–2363.
- V. T. Tiong, N. D. Pham, T. Wang, T. X. Zhu, X. L. Zhao, Y. H. Zhang, Q. Shen, J. Bell, L. H. Hu, S. Y. Dai and H. X. Wang, *Adv. Funct. Mater.*, 2018, **28**, 14.
- C. Eames, J. M. Frost, P. R. F. Barnes, B. C. O'Regan, A. Walsh and M. S. Islam, *Nat. Commun.*, 2015, **6**, 7497.
- A. Senocrate, I. Moudrakovski, G. Y. Kim, T.-Y. Yang, G. Gregori, M. Grätzel and J. Maier, *Angew. Chem., Int. Ed.*, 2017, **56**, 7755–7759.
- W. Peng, C. Aranda, O. M. Bakr, G. Garcia-Belmonte, J. Bisquert and A. Guerrero, *ACS Energy Lett.*, 2018, **3**, 1477–1481.
- C. Li, A. Guerrero, S. Hüttner and J. Bisquert, *Nat. Commun.*, 2018, **9**, 5113.
- L. M. Herz, *ACS Energy Lett.*, 2017, **2**, 1539–1548.
- N. Vicente and G. Garcia-Belmonte, *Adv. Energy Mater.*, 2017, **7**, 1700710.
- S. A. L. Weber, I. M. Hermes, S. H. Turren-Cruz, C. Gort, V. W. Bergmann, L. Gilson, A. Hagfeldt, M. Graetzel, W. Tress and R. Berger, *Energy Environ. Sci.*, 2018, **11**, 2404–2413.
- F. Fu, T. Feurer, T. Jäger, E. Avancini, B. Bissig, S. Yoon, S. Buecheler and A. N. Tiwari, *Nat. Commun.*, 2015, **6**, 8932.
- O. Almora, C. Aranda and G. Garcia-Belmonte, *J. Phys. Chem. C*, 2018, **122**, 13450–13454.
- Z. Zolfaghari, E. Hassanabadi, D. Pitarch-Tena, S. J. Yoon, Z. Shariatinia, J. van de Lagemaat, J. M. Luther and I. Mora-Seró, *ACS Energy Lett.*, 2019, **4**, 251–258.
- I. Zarazua, G. Han, P. P. Boix, S. Mhaisalkar, F. Fabregat-Santiago, I. Mora-Seró, J. Bisquert and G. Garcia-Belmonte, *J. Phys. Chem. Lett.*, 2016, **7**, 5105–5113.
- O. Almora, A. Guerrero and G. Garcia-Belmonte, *Appl. Phys. Lett.*, 2016, **108**, 043903.
- J. Bisquert, *Nanostructured Energy Devices: Equilibrium Concepts and Kinetics*, CRC Press, Boca Raton, 2014.
- A. Guerrero, G. Garcia-Belmonte, I. Mora-Sero, J. Bisquert, Y. S. Kang, T. J. Jacobsson, J.-P. Correa-Baena and A. Hagfeldt, *J. Phys. Chem. C*, 2016, **120**, 8023–8032.
- I. Zarazua, J. Bisquert and G. Garcia-Belmonte, *J. Phys. Chem. Lett.*, 2016, **7**, 525–528.
- H.-S. Kim, I.-H. Jang, N. Ahn, M. Choi, A. Guerrero, J. Bisquert and N.-G. Park, *J. Phys. Chem. Lett.*, 2015, **6**, 4633–4639.
- O. Almora, C. Aranda, I. Zarazua, A. Guerrero and G. Garcia-Belmonte, *ACS Energy Lett.*, 2016, **1**, 209–215.
- V. K. Sangwan, M. Zhu, S. Clark, K. A. Luck, T. J. Marks, M. G. Kanatzidis and M. C. Hersam, *ACS Appl. Mater. Interfaces*, 2019, **11**, 14166–14174.
- O. Almora, I. Zarazua, E. Mas-Marza, I. Mora-Sero, J. Bisquert and G. Garcia-Belmonte, *J. Phys. Chem. Lett.*, 2015, **6**, 1645–1652.
- Y. G. Rong, Y. Hu, S. Ravishankar, H. W. Liu, X. M. Hou, Y. S. Sheng, A. Y. Mei, Q. F. Wang, D. Y. Li, M. Xu, J. Bisquert and H. W. Han, *Energy Environ. Sci.*, 2017, **10**, 2383–2391.
- A. Guerrero, E. J. Juarez-Perez, J. Bisquert, I. Mora-Sero and G. Garcia-Belmonte, *Appl. Phys. Lett.*, 2014, **105**, 133902.
- O. Almora, C. Aranda, E. Mas-Marzá and G. Garcia-Belmonte, *Appl. Phys. Lett.*, 2016, **109**, 173903.
- D. Liu, Q. Wang, C. J. Traverse, C. Yang, M. Young, P. S. Kuttipillai, S. Y. Lunt, T. W. Hamann and R. R. Lunt, *ACS Nano*, 2018, **12**, 876–883.
- C. Aranda, A. Guerrero and J. Bisquert, *ACS Energy Lett.*, 2019, **4**, 741–746.
- C. S. Ponceca, T. J. Savenije, M. Abdellah, K. Zheng, A. Yartsev, T. Pascher, T. Harlang, P. Chabera, T. Pullerits, A. Stepanov, J.-P. Wolf and V. Sundström, *J. Am. Chem. Soc.*, 2014, **136**, 5189–5192.

- 43 S. van Reenen, M. Kemerink and H. J. Snaith, *J. Phys. Chem. Lett.*, 2015, **6**, 3808–3814.
- 44 P. Schulz, E. Edri, S. Kirmayer, G. Hodes, D. Cahen and A. Kahn, *Energy Environ. Sci.*, 2014, **7**, 1377–1381.
- 45 G. Yang, C. Wang, H. Lei, X. Zheng, P. Qin, L. Xiong, X. Zhao, Y. Yan and G. Fang, *J. Mater. Chem. A*, 2017, **5**, 1658–1666.
- 46 C. Quarti, F. De Angelis and D. Beljonne, *Chem. Mater.*, 2017, **29**, 958–968.
- 47 F. Zu, P. Amsalem, M. Ralaiarisoa, T. Schultz, R. Schlesinger and N. Koch, *ACS Appl. Mater. Interfaces*, 2017, **9**, 41546–41552.
- 48 S. Wang, T. Sakurai, W. Wen and Y. Qi, *Adv. Mater. Interfaces*, 2018, **5**, 1800260.
- 49 E. M. Miller, Y. Zhao, C. C. Mercado, S. K. Saha, J. M. Luther, K. Zhu, V. Stevanović, C. L. Perkins and J. van de Lagemaat, *Phys. Chem. Chem. Phys.*, 2014, **16**, 22122–22130.
- 50 D. Liu, S. Li, P. Zhang, Y. Wang, R. Zhang, H. Sarvari, F. Wang, J. Wu, Z. Wang and Z. D. Chen, *Nano Energy*, 2017, **31**, 462–468.
- 51 H. Tan, A. Jain, O. Voznyy, X. Lan, F. P. García de Arquer, J. Z. Fan, R. Quintero-Bermudez, M. Yuan, B. Zhang, Y. Zhao, F. Fan, P. Li, L. N. Quan, Y. Zhao, Z.-H. Lu, Z. Yang, S. Hoogland and E. H. Sargent, *Science*, 2017, **355**, 722.
- 52 F. Giordano, A. Abate, J. P. Correa Baena, M. Saliba, T. Matsui, S. H. Im, S. M. Zakeeruddin, M. K. Nazeeruddin, A. Hagfeldt and M. Graetzel, *Nat. Commun.*, 2016, **7**, 10379.
- 53 J. Wang, M. Qin, H. Tao, W. Ke, Z. Chen, J. Wan, P. Qin, L. Xiong, H. Lei, H. Yu and G. Fang, *Appl. Phys. Lett.*, 2015, **106**, 121104.
- 54 J.-Y. Seo, R. Uchida, H.-S. Kim, Y. Saygili, J. Luo, C. Moore, J. Kerrod, A. Wagstaff, M. Eklund, R. McIntyre, N. Pellet, S. M. Zakeeruddin, A. Hagfeldt and M. Grätzel, *Adv. Funct. Mater.*, 2018, **28**, 1705763.
- 55 N. D. Pham, C. Zhang, V. T. Tiong, S. Zhang, G. Will, A. Bou, J. Bisquert, P. E. Shaw, A. Du, G. J. Wilson and H. Wang, *Adv. Funct. Mater.*, 2019, **29**, 1806479.
- 56 C. H. Ng, T. S. Ripples, K. Hamada, S. H. Teo, H. N. Lim, J. Bisquert and S. Hayase, *Sci. Rep.*, 2018, **8**, 2482.
- 57 S. Fantacci, F. De Angelis, M. K. Nazeeruddin and M. Grätzel, *J. Phys. Chem. C*, 2011, **115**, 23126–23133.
- 58 I. Gelmetti, N. F. Montcada, A. Pérez-Rodríguez, E. Barrena, C. Ocal, I. García-Benito, A. Molina-Ontoria, N. Martín, A. Vidal-Ferran and E. Palomares, *Energy Environ. Sci.*, 2019, **12**, 1309.
- 59 S. Ravishankar, S. Gharibzadeh, C. Roldán-Carmona, G. Grancini, Y. Lee, M. Ralaiarisoa, A. M. Asiri, N. Koch, J. Bisquert and M. K. Nazeeruddin, *Joule*, 2018, **2**, 788–798.
- 60 R. Gottesman, P. Lopez-Varo, L. Gouda, J. A. Jimenez-Tejada, J. Hu, S. Tirosh, A. Zaban and J. Bisquert, *Chem.*, 2016, **1**, 776–789.
- 61 M. García-Rosell, A. Bou, J. A. Jiménez-Tejada, J. Bisquert and P. Lopez-Varo, *J. Phys. Chem. C*, 2018, **122**, 13920–13925.
- 62 A. Guerrero, A. Bou, G. Matt, O. Almora, T. Heumüller, G. Garcia-Belmonte, J. Bisquert, Y. Hou and C. Brabec, *Adv. Energy Mater.*, 2018, **8**, 1703376.
- 63 S. Ravishankar, O. Almora, C. Echeverría-Arrondo, E. Ghahremanirad, C. Aranda, A. Guerrero, F. Fabregat-Santiago, A. Zaban, G. Garcia-Belmonte and J. Bisquert, *J. Phys. Chem. Lett.*, 2017, **8**, 915–921.
- 64 E. Ghahremanirad, A. Bou, S. Olyae and J. Bisquert, *J. Phys. Chem. Lett.*, 2017, **8**, 1402–1406.
- 65 A. Zohar, N. Kedem, I. Levine, D. Zohar, A. Vilan, D. Ehre, G. Hodes and D. Cahen, *J. Phys. Chem. Lett.*, 2016, **7**, 191–197.
- 66 M. Anaya, W. Zhang, B. C. Hames, Y. Li, F. Fabregat-Santiago, M. E. Calvo, H. J. Snaith, H. Miguez and I. Mora-Sero, *J. Mater. Chem. C*, 2017, **5**, 634–644.
- 67 D. Moia, I. Gelmetti, P. Calado, W. Fisher, M. Stringer, O. Game, Y. Hu, P. Docampo, D. Lidzey, E. Palomares, J. Nelson and P. R. F. Barnes, *Energy Environ. Sci.*, 2019, **12**, 1296.
- 68 F. Ebadi, N. Taghavinia, R. Mohammadpour, A. Hagfeldt and W. Tress, *Nat. Commun.*, 2019, **10**, 1574.
- 69 D. A. Jacobs, H. Shen, F. Pfeffer, J. Peng, T. P. White, F. J. Beck and K. R. Catchpole, *J. Appl. Phys.*, 2018, **124**, 225702.
- 70 A. Pockett and M. J. Carnie, *ACS Energy Lett.*, 2017, **2**, 1683–1689.
- 71 M. Ershov, H. C. Liu, L. Li, M. Buchanan, Z. R. Wasilevski and A. K. Jonsher, *IEEE Trans. Electron Devices*, 1998, **45**, 2196.
- 72 I. Mora-Seró, J. Bisquert, F. Fabregat-Santiago, G. Garcia-Belmonte, G. Zoppi, K. Durose, Y. Y. Proskuryakov, I. Oja, A. Belaidi, T. Dittrich, R. Tena-Zaera, A. Katty, C. Lévy-Clement, V. Barrio and S. J. C. Irvine, *Nano Lett.*, 2006, **6**, 640–650.
- 73 F. Fabregat-Santiago, M. Kulbak, A. Zohar, M. Vallés-Pelarda, G. Hodes, D. Cahen and I. Mora-Seró, *ACS Energy Lett.*, 2017, **2**, 2007–2013.
- 74 J. Bisquert, G. Garcia-Belmonte, A. Pitarch and H. Bolink, *Chem. Phys. Lett.*, 2006, **422**, 184–191.
- 75 J. Bisquert, *Phys. Chem. Chem. Phys.*, 2011, **13**, 4679–4685.
- 76 R. M. L. Evans, *Phys. Rev. Lett.*, 2004, **92**, 150601.
- 77 A. Pockett, G. E. Eperon, T. Peltola, H. J. Snaith, A. B. Walker, L. M. Peter and P. J. Cameron, *J. Phys. Chem. C*, 2015, **119**, 3456–3465.
- 78 L. Bertoluzzi and J. Bisquert, *J. Phys. Chem. Lett.*, 2017, **8**, 172–180.
- 79 S. Ravishankar, C. Aranda, S. Sanchez, J. Bisquert, M. Saliba and G. Garcia-Belmonte, *J. Phys. Chem. C*, 2019, **123**, 6444–6449.
- 80 V. W. Bergmann, Y. Guo, H. Tanaka, I. M. Hermes, D. Li, A. Klasen, S. A. Bretschneider, E. Nakamura, R. Berger and S. A. L. Weber, *ACS Appl. Mater. Interfaces*, 2016, **8**, 19402–19409.
- 81 W. Zhou, Y. Zhao, X. Zhou, R. Fu, Q. Li, Y. Zhao, K. Liu, D. Yu and Q. Zhao, *J. Phys. Chem. Lett.*, 2017, **8**, 4122–4128.
- 82 Y. Feng, Y. Zhao, W.-K. Zhou, Q. Li, W. A. Saidi, Q. Zhao and X.-Z. Li, *J. Phys. Chem. Lett.*, 2018, **9**, 6536–6543.
- 83 K. Domanski, B. Roose, T. Matsui, M. Saliba, S.-H. Turren-Cruz, J.-P. Correa-Baena, C. R. Carmona, G. Richardson,

- J. M. Foster, F. De Angelis, J. M. Ball, A. Petrozza, N. Mine, M. K. Nazeeruddin, W. Tress, M. Grätzel, U. Steiner, A. Hagfeldt and A. Abate, *Energy Environ. Sci.*, 2017, **10**, 604–613.
- 84 J. Carrillo, A. Guerrero, S. Rahimnejad, O. Almora, I. Zarazua, E. Mas-Marza, J. Bisquert and G. Garcia-Belmonte, *Adv. Energy Mater.*, 2016, **6**, 1502246.
- 85 M. Z. Bazant, K. Thornton and A. Ajdari, *Phys. Rev. E: Stat., Nonlinear, Soft Matter Phys.*, 2004, **70**, 021506.
- 86 W.-J. Yin, T. Shi and Y. Yan, *Appl. Phys. Lett.*, 2014, **104**, 063903.
- 87 J. M. Frost, K. T. Butler, F. Brivio, C. H. Hendon, M. van Schilfgaarde and A. Walsh, *Nano Lett.*, 2014, **14**, 2584–2590.
- 88 P. Umari, E. Mosconi and F. De Angelis, *Sci. Rep.*, 2014, **4**, 4467.
- 89 C.-J. Yu, *J. Phys.: Energy*, 2019, **1**, 022001.
- 90 D. Meggiolaro, E. Mosconi and F. De Angelis, *ACS Energy Lett.*, 2018, **3**, 447–451.
- 91 H. Uratani and K. Yamashita, *J. Phys. Chem. Lett.*, 2017, **8**, 742–746.
- 92 J. M. Azpiroz, E. Mosconi, J. Bisquert and F. De Angelis, *Energy Environ. Sci.*, 2015, **8**, 2118–2127.
- 93 E. Mosconi, E. Ronca and F. De Angelis, *J. Phys. Chem. Lett.*, 2014, **5**, 2619–2625.
- 94 M. Coll, A. Gomez, E. Mas-Marza, O. Almora, G. Garcia-Belmonte, M. Campoy-Quiles and J. Bisquert, *J. Phys. Chem. Lett.*, 2015, **6**, 1408–1413.
- 95 Y. Rakita, O. Bar-Elli, E. Meirzadeh, H. Kaslasi, Y. Peleg, G. Hodes, I. Lubomirsky, D. Oron, D. Ehre and D. Cahen, *Proc. Natl. Acad. Sci. U. S. A.*, 2017, **114**, E5504–E5512.
- 96 L. M. Garten, D. T. Moore, S. U. Nanayakkara, S. Dwaraknath, P. Schulz, J. Wands, A. Rockett, B. Newell, K. A. Persson, S. Trolier-McKinstry and D. S. Ginley, *Sci. Adv.*, 2019, **5**, eaas9311.
- 97 H. Röhm, T. Leonhard, M. J. Hoffmann and A. Colsmann, *Energy Environ. Sci.*, 2017, **10**, 950–955.
- 98 Q. Zhang, A. Solanki, K. Parida, D. Giovanni, M. Li, T. L. C. Jansen, M. S. Pshenichnikov and T. C. Sum, *ACS Appl. Mater. Interfaces*, 2019, **11**, 13523–13532.
- 99 P. Lopez-Varo, L. Bertoluzzi, J. Bisquert, M. Alexe, M. Coll, J. Huang, J. A. Jimenez-Tejada, T. Kirchartz, R. Nechache, F. Rosei and Y. Yuan, *Phys. Rep.*, 2016, **653**, 1–40.
- 100 Y. S. Yang, S. J. Lee, S. Yi, B. G. Chae, S. H. Lee, H. J. Joo and M. S. Jang, *Appl. Phys. Lett.*, 2000, **76**, 774–776.
- 101 G.-L. Yuan and J. Wang, *Appl. Phys. Lett.*, 2009, **95**, 252904.
- 102 Y. Yuan, T. J. Reece, P. Sharma, S. Poddar, S. Ducharme, A. Gruverman, Y. Yang and J. Huang, *Nat. Mater.*, 2011, **10**, 296–302.
- 103 K. Asadi, P. de Bruyn, P. W. M. Blom and D. M. de Leeuw, *Appl. Phys. Lett.*, 2011, **98**, 183301.
- 104 A. Pérez-Tomas, H. Xie, Z. Wang, H.-S. Kim, I. Shirley, S.-H. Turren-Cruz, A. Morales-Melgares, B. Saliba, D. Tanenbaum, M. Saliba, S. M. Zakeeruddin, M. Gratzel, A. Hagfeldt and M. Lira-Cantu, *Sustainable Energy Fuels*, 2019, **3**, 382–389.
- 105 Y. Yang, N. D. Pham, D. S. Yao, H. Y. Zhu, P. Yarlagadda and H. X. Wang, *Chin. Chem. Lett.*, 2018, **29**, 1242–1250.
- 106 L. Cojocaru, S. Uchida, P. V. V. Jayaweera, S. Kaneko, H. B. Wang, J. Nakazaki, T. Kubo and H. Segawa, *Energy Technol.*, 2017, **5**, 1762–1766.
- 107 T. W. Kim, M. Kim, L. Cojocaru, S. Uchida and H. Segawa, *ACS Energy Lett.*, 2018, **3**, 2743–2749.
- 108 A. Guerrero, J. You, C. Aranda, Y. S. Kang, G. Garcia-Belmonte, H. Zhou, J. Bisquert and Y. Yang, *ACS Nano*, 2016, **10**, 218–224.
- 109 Y. Kato, L. K. Ono, M. V. Lee, S. Wang, S. R. Raga and Y. Qi, *Adv. Mater. Interfaces*, 2015, **2**, 1500195.
- 110 V. Verdingovas, L. Müller, M. S. Jellesen, F. B. Grumsen and R. Ambat, *Corros. Sci.*, 2015, **97**, 161–171.
- 111 K. Domanski, J.-P. Correa-Baena, N. Mine, M. K. Nazeeruddin, A. Abate, M. Saliba, W. Tress, A. Hagfeldt and M. Grätzel, *ACS Nano*, 2016, **10**, 6306–6314.
- 112 M. Kaltenbrunner, G. Adam, E. D. Glowacki, M. Drack, R. Schwodauer, L. Leonat, D. H. Apaydin, H. Groiss, M. C. Scharber, M. S. White, N. S. Sariciftci and S. Bauer, *Nat. Mater.*, 2015, **14**, 1032–1039.
- 113 J. T. Tisdale, E. Muckley, M. Ahmadi, T. Smith, C. Seal, E. Lukosi, I. N. Ivanov and B. Hu, *Adv. Mater. Interfaces*, 2018, **5**, 7.
- 114 W. Peng, L. F. Wang, B. Murali, K. T. Ho, A. Bera, N. Cho, C. F. Kang, V. M. Burlakov, J. Pan, L. Sinatra, C. Ma, W. Xu, D. Shi, E. Alarousu, A. Goriely, H. He, O. F. Mohammed, T. Wu and O. M. Bakr, *Adv. Mater.*, 2016, **28**, 3383–3390.
- 115 J. H. Heo, M. S. You, M. H. Chang, W. Yin, T. K. Ahn, S.-J. Lee, S.-J. Sung, D. H. Kim and S. H. Im, *Nano Energy*, 2015, **15**, 530–539.
- 116 S. Wang, B. Liu, Y. Zhu, Z. Ma, B. Liu, X. Miao, R. Ma and C. Wang, *Sol. Energy*, 2018, **169**, 335–342.
- 117 X. Gu, Y. Wang, T. Zhang, D. Liu, R. Zhang, P. Zhang, J. Wu, Z. D. Chen and S. Li, *J. Mater. Chem. C*, 2017, **5**, 10754–10760.
- 118 J. K. Kim, S. U. Chai, Y. Ji, B. Levy-Wendt, S. H. Kim, Y. Yi, T. F. Heinz, J. K. Nørskov, J. H. Park and X. Zheng, *Adv. Energy Mater.*, 2018, **8**, 1801717.
- 119 M. Li, Y. Huan, X. Yan, Z. Kang, Y. Guo, Y. Li, X. Liao, R. Zhang and Y. Zhang, *ChemSusChem*, 2018, **11**, 171–177.
- 120 Y. Li, Y. Guo, Y. Li and X. Zhou, *Electrochim. Acta*, 2016, **200**, 29–36.
- 121 X.-X. Gao, Q.-Q. Ge, D.-J. Xue, J. Ding, J.-Y. Ma, Y.-X. Chen, B. Zhang, Y. Feng, L.-J. Wan and J.-S. Hu, *Nanoscale*, 2016, **8**, 16881–16885.
- 122 Y. Xiang, Z. Ma, J. Zhuang, H. Lu, C. Jia, J. Luo, H. Li and X. Cheng, *J. Phys. Chem. C*, 2017, **121**, 20150–20157.
- 123 C. Liang, P. Li, Y. Zhang, H. Gu, Q. Cai, X. Liu, J. Wang, H. Wen and G. Shao, *J. Power Sources*, 2017, **372**, 235–244.
- 124 Z. Ren, J. Wu, N. Wang and X. Li, *J. Mater. Chem. A*, 2018, **6**, 15348–15358.
- 125 R. Ranjan, A. Prakash, A. Singh, A. Singh, A. Garg and R. K. Gupta, *J. Mater. Chem. A*, 2018, **6**, 1037–1047.
- 126 L.-L. Jiang, Z.-K. Wang, M. Li, C.-H. Li, P.-F. Fang and L.-S. Liao, *Sol. RRL*, 2018, 1800149.
- 127 H.-H. Wang, Q. Chen, H. Zhou, L. Song, Z. S. Louis, N. D. Marco, Y. Fang, P. Sun, T.-B. Song, H. Chen and Y. Yang, *J. Mater. Chem. A*, 2015, **3**, 9108–9115.

- 128 H. Liu, Z. Zhang, X. Zhang, Y. Cai, Y. Zhou, Q. Qin, X. Lu, X. Gao, L. Shui, S. Wu and J.-M. Liu, *Electrochim. Acta*, 2018, **272**, 68–76.
- 129 J. Peng, T. Duong, X. Zhou, H. Shen, Y. Wu, H. K. Mulmudi, Y. Wan, D. Zhong, J. Li, T. Tsuzuki, K. J. Weber, K. R. Catchpole and T. P. White, *Adv. Energy Mater.*, 2017, **7**, 1601768.
- 130 Q. Cai, Y. Zhang, C. Liang, P. Li, H. Gu, X. Liu, J. Wang, Z. Shentu, J. Fan and G. Shao, *Electrochim. Acta*, 2018, **261**, 227–235.
- 131 F. Giordano, A. Abate, J. P. C. Baena, M. Saliba, T. Matsui, S. H. Im, S. M. Zakeeruddin, M. K. Nazeeruddin, A. Hagfeldt and M. Graetzel, *Nat. Commun.*, 2016, **7**, 10379.
- 132 D. S. Yao, C. M. Zhang, N. D. Pham, Y. H. Zhang, V. T. Tiong, A. J. Du, Q. Shen, G. J. Wilson and H. X. Wang, *J. Phys. Chem. Lett.*, 2018, **9**, 2113–2120.
- 133 V. Zardetto, F. di Giacomo, H. Lifka, M. A. Verheijen, C. H. L. Weijtens, L. E. Black, S. Veenstra, W. M. M. Kessels, R. Andriessen and M. Creatore, *Adv. Mater. Interfaces*, 2018, **5**, 6.
- 134 J. P. Correa-Baena, L. Steier, W. Tress, M. Saliba, S. Neutzner, T. Matsui, F. Giordano, T. J. Jacobsson, A. R. Srimath Kandada, S. M. Zakeeruddin, A. Petrozza, A. Abate, M. K. Nazeeruddin, M. Gratzel and A. Hagfeldt, *Energy Environ. Sci.*, 2015, **8**, 2928–2934.
- 135 T. Hu, T. Becker, N. Pourdavoud, J. Zhao, K. O. Brinkmann, R. Heiderhoff, T. Gahlmann, Z. Huang, S. Olthof, K. Meerholz, D. Többens, B. Cheng, Y. Chen and T. Riedl, *Adv. Mater.*, 2017, **29**, 1606656.
- 136 M. M. Tavakoli, P. Yadav, R. Tavakoli and J. Kong, *Adv. Energy Mater.*, 2018, **8**, 9.
- 137 C. Di Valentin, G. Pacchioni and A. Selloni, *J. Phys. Chem. C*, 2009, **113**, 20543–20552.
- 138 H. Schmidt, K. Zilberberg, S. Schmale, H. Flügge, T. Riedl and W. Kowalsky, *Appl. Phys. Lett.*, 2010, **96**, 243305.
- 139 A. Guerrero, S. Chambon, L. Hirsch and G. Garcia-Belmonte, *Adv. Funct. Mater.*, 2014, **24**, 6234–6240.
- 140 R. A. Kerner and B. P. Rand, *J. Phys. Chem. Lett.*, 2017, **8**, 2298–2303.
- 141 K. K. Wong, A. Fakharuddin, P. Ehrenreich, T. Deckert, M. Abdi-Jalebi, R. H. Friend and L. Schmidt-Mende, *J. Phys. Chem. C*, 2018, **122**, 10691–10698.
- 142 J. Will, Y. Hou, S. Scheiner, U. Pinkert, I. M. Hermes, S. A. L. Weber, A. Hirsch, M. Halik, C. Brabec and T. Unruh, *ACS Appl. Mater. Interfaces*, 2018, **10**, 5511–5518.
- 143 X. Liu, Y. F. Zhang, L. Shi, Z. H. Liu, J. L. Huang, J. S. Yun, Y. Y. Zeng, A. B. Pu, K. W. Sun, Z. Hameiri, J. A. Stride, J. Seidel, M. A. Green and X. J. Hao, *Adv. Energy Mater.*, 2018, **8**, 1800138.
- 144 L. J. Zuo, Q. Chen, N. De Marco, Y. T. Hsieh, H. J. Chen, P. Y. Sun, S. Y. Chang, H. X. Zhao, S. Q. Dong and Y. Yang, *Nano Lett.*, 2017, **17**, 269–275.
- 145 J. Peng, Y. Wu, W. Ye, D. A. Jacobs, H. Shen, X. Fu, Y. Wan, T. Duong, N. Wu, C. Barugkin, H. T. Nguyen, D. Zhong, J. Li, T. Lu, Y. Liu, M. N. Lockrey, K. J. Weber, K. R. Catchpole and T. P. White, *Energy Environ. Sci.*, 2017, **10**, 1792–1800.
- 146 J. B. Patel, J. Wong-Leung, S. Van Reenen, N. Sakai, J. T. W. Wang, E. S. Parrott, M. Z. Liu, H. J. Snaith, L. M. Herz and M. B. Johnston, *Adv. Electron. Mater.*, 2017, **3**, 6.
- 147 F. Ali, N. D. Pham, H. J. Bradford, N. Khoshirsat, K. Ostrikov, J. M. Bell, H. Wang and T. Tesfamichael, *ChemSusChem*, 2018, **11**, 3096–3103.
- 148 A. Mei, X. Li, L. Liu, Z. Ku, T. Liu, Y. Rong, M. Xu, M. Hu, J. Chen, Y. Yang, M. Grätzel and H. Han, *Science*, 2014, **345**, 295–298.
- 149 U. B. Cappel, T. Daeneke and U. Bach, *Nano Lett.*, 2012, **12**, 4925–4931.
- 150 R. S. Sanchez and E. Mas-Marza, *Sol. Energy Mater. Sol. Cells*, 2016, **158**, 189–194.
- 151 Z. Li, C. Xiao, Y. Yang, S. P. Harvey, D. H. Kim, J. A. Christians, M. Yang, P. Schulz, S. U. Nanayakkara, C.-S. Jiang, J. M. Luther, J. J. Berry, M. C. Beard, M. M. Al-Jassim and K. Zhu, *Energy Environ. Sci.*, 2017, **10**, 1234–1242.
- 152 Z. Li, C. X. Xiao, Y. Yang, S. P. Harvey, D. H. Kim, J. A. Christians, M. J. Yang, P. Schulz, S. U. Nanayakkara, C. S. Jiang, J. M. Luther, J. J. Berry, M. C. Beard, M. M. Al-Jassim and K. Zhu, *Energy Environ. Sci.*, 2017, **10**, 1234–1242.
- 153 S. P. Harvey, Z. Li, J. A. Christians, K. Zhu, J. M. Luther and J. J. Berry, *ACS Appl. Mater. Interfaces*, 2018, **10**, 28541–28552.
- 154 Y. F. Yue, N. Salim, Y. Z. Wu, X. D. Yang, A. Islam, W. Chen, J. Liu, E. B. Bi, F. X. Xie, M. L. Cai and L. Y. Han, *Adv. Mater.*, 2016, **28**, 10738.
- 155 T. H. Schloemer, T. S. Gehan, J. A. Christians, D. G. Mitchell, A. Dixon, Z. Li, K. Zhu, J. J. Berry, J. M. Luther and A. Sellinger, *ACS Energy Lett.*, 2019, **4**, 473–482.
- 156 Y. Hou, X. Du, S. Scheiner, D. P. McMeekin, Z. Wang, N. Li, M. S. Killian, H. Chen, M. Richter, I. Levchuk, N. Schrenker, E. Specker, T. Stubhan, N. A. Luechinger, A. Hirsch, P. Schmuki, H.-P. Steinrück, R. H. Fink, M. Halik, H. J. Snaith and C. J. Brabec, *Science*, 2017, **358**, 1192–1197.
- 157 E. M. Sanehira, B. J. Tremolet de Villers, P. Schulz, M. O. Reese, S. Ferrere, K. Zhu, L. Y. Lin, J. J. Berry and J. M. Luther, *ACS Energy Lett.*, 2016, **1**, 38–45.
- 158 P. Schulz, J. O. Tiepelt, J. A. Christians, I. Levine, E. Edri, E. M. Sanehira, G. Hodes, D. Cahen and A. Kahn, *ACS Appl. Mater. Interfaces*, 2016, **8**, 31491–31499.
- 159 M. Shahbazi and H. X. Wang, *Sol. Energy*, 2016, **123**, 74–87.
- 160 N. Sultana, N. J. Demarais, D. Shevchenko and P. J. Derrick, *Sol. RRL*, 2018, **2**, 9.